Geophysical Research Letters

RESEARCH LETTER
10.1029/2020GL087101

Key Points:
- Land-atmosphere coupling embeds surface controls on ET in the atmospheric state
- We evaluate a simple equation for actual ET, with no parameters or surface inputs
- Across 76 sites, errors in the equation's predictions are comparable to those in eddy covariance data

Supporting Information:
- Supporting Information S1

Correspondence to:
K. A. McColl,
kmccoll@seas.harvard.edu

Citation:
McColl, K. A., & Rigden, A. J. (2020). Emergent simplicity of continental evapotranspiration. *Geophysical Research Letters*, *47*, e2020GL087101. https://doi.org/10.1029/2020GL087101

Received 14 JAN 2020
Accepted 5 MAR 2020
Accepted article online 13 MAR 2020

Emergent Simplicity of Continental Evapotranspiration

Kaighin A. McColl[1,2] **and Angela J. Rigden**[1]

[1]Department of Earth and Planetary Sciences, Harvard University, Cambridge, MA, USA, [2]School of Engineering and Applied Sciences, Harvard University, Cambridge, MA, USA

Abstract Evapotranspiration (ET) is challenging to model because it depends on heterogeneous land surface features—such as soil moisture, land cover type, and plant physiology—resulting in rising model complexity and substantial disagreement between models. We show that the evaporative fraction (ET as a proportion of available energy at the surface) can be estimated accurately across a broad range of conditions using a simple equation with no free parameters and no land surface information; only near-surface air temperature and specific humidity observations are required. The equation performs well when compared to eddy covariance measurements at 76 inland continental sites, with prediction errors comparable to errors in the eddy covariance measurements themselves, despite substantial variability in surface conditions across sites. This reveals an emergent simplicity to continental ET that has not been previously recognized, in which land-atmosphere coupling efficiently embeds land surface information in the near-surface atmospheric state on daily to monthly time scales.

1. Introduction

Evapotranspiration (ET, the sum of evaporation and transpiration) is a key flux in the terrestrial water, energy, and carbon cycles. As a component of the water cycle, it is of fundamental importance to water resource management, agriculture, and ecosystem health. As a substantial flux of latent heat in the land surface energy budget, it effectively cools the near-surface atmosphere. Plants make trade-offs between transpiration and photosynthesis through stomatal regulation, which directly impacts the terrestrial carbon budget (Friedlingstein et al., 2013; Green et al., 2019). Since ET coregulates the water, energy, and carbon cycles, changes in any one cycle that impact ET can potentially propagate through the other cycles. However, ET has only been measured on a routine basis since the 1990s, and measurements are relatively sparse due to the high cost of installing and maintaining eddy covariance instruments. As a result, ET models remain essential for characterizing ET at regional and global scales.

The land surface strongly constrains ET (Monteith, 1965) but is challenging to model due to its heterogeneity. In an attempt to represent this heterogeneity, land surface models have become increasingly complex (Sellers et al., 1997), at the cost of introducing additional parameters, which are difficult to constrain at global scales. For example, one key parameter in modeling ET—the stomatal conductance g_s—is often itself parameterized (Ball et al., 1987) as a function of relative humidity, atmospheric CO_2 concentration, and photosynthetic assimilation rate (A). This scheme includes two parameters and also requires a separate parameterization of A; one common scheme (Farquhar et al., 1980) for A requires at least another four parameters. In addition, the impact of water limitation on ET is often imposed by multiplying g_s by an empirical function of soil moisture, varying between 0 and 1, requiring at least another two parameters (Trugman et al., 2018). Most of these parameters further vary between, and within, plant functional types. Constraining these and other parameters relevant to ET is a major challenge in land surface modeling. As a result, global models struggle to represent ET with high accuracy (Mueller & Seneviratne, 2014), particularly over inland continental regions (Ma et al., 2018).

A growing body of evidence suggests that modeling continental ET may be simpler than it first appears. Over many land surfaces, strong coupling between the land and atmosphere mean the land surface state becomes embedded in the atmospheric state at daily or longer time scales (Bouchet, 1963; Morton, 1969; McColl et al., 2019; Novick et al., 2016; Salvucci & Gentine, 2013; Zhou et al., 2019), implying that atmospheric observations alone should contain sufficient information to estimate ET. This is potentially useful because it implies that ET can be measured or modeled without explicitly measuring or modeling the land surface,

the source of many modeling errors. Various methods have exploited this relation and have been empirically successful in estimating ET while using relatively little land surface information (Brondani et al., 2019; Gentine et al., 2013, 2016; Rigden & Salvucci, 2015; Salvucci & Gentine, 2013, 2015).

While theoretically possible, extracting the ET signal solely from atmospheric observations has proven more challenging. Methods for estimating ET over water-limited land surfaces almost always require at least some land surface information: At minimum, semiempirical surface roughness and stratified turbulence parameterizations are required, which typically require observations of vegetation height and wind speed (Gentine et al., 2016; Rigden & Salvucci, 2015; Salvucci & Gentine, 2013). The semiempirical parameterizations include parameters that are substantially uncertain and vary with plant functional type (Rigden et al., 2018), so their elimination is also desirable. Schemes for estimating ET from satellite observations also require at least some land surface inputs, such as visible, near-infrared, and/or thermal infrared radiances (Anderson et al., 2011; Bastiaanssen et al., 1998; Fisher et al., 2008; Mu et al., 2011) or observations of soil moisture and vegetation water content (Miralles et al., 2011).

A recent study (McColl et al., 2019) hypothesized that, in many inland continental regions, the near-surface atmosphere is in a state of "surface flux equilibrium" (SFE), in which the surface moistening and surface heating terms in the near-surface relative humidity budget approximately balance. On daily to monthly time scales, the theory predicts that the Bowen ratio, $B = \frac{H}{\lambda E}$, can be estimated as

$$B \approx \frac{R_v c_p T_a^2}{\lambda^2 q_a} \tag{1}$$

where λE and H are the latent and sensible heat fluxes (W m^{-2}), respectively, q_a is screen-level specific humidity (-), T_a is screen-level air temperature (K), $\lambda = 2.5008 \times 10^6$ (J kg^{-1}) is the latent heat of vaporization of water, $c_p = 1,005$ (J kg^{-1} K^{-1}) is the specific heat capacity of air at constant pressure, and $R_v = 461.5$ (J kg^{-1} K^{-1}) is the gas constant for water vapor. Here, all quantities that vary in time are daily (i.e., a 24-hr period) or monthly averages. The Bowen ratio can be converted to latent heat flux using the relation $\lambda E = (1 + B)^{-1}(R_n - G)$, where $(1 + B)^{-1}$ is the "evaporative fraction" (EF), R_n is net radiation at the surface (W m^{-2}), and G is ground heat flux (W m^{-2}). G is typically small compared to R_n at daily or longer time scales and is often ignored.

Unlike previous approaches, this model of water-limited B has zero free parameters, does not require any land surface information as inputs (including vegetation height), and does not require wind speed. Two lines of evidence were given for the validity of this theory. First, a simple steady-state box model of the atmosphere, coupled to a land surface, reproduced SFE across a wide range of plausible conditions. Second, it was shown analytically that, under steady conditions, equation (1) is exactly equivalent to a recent method—the Evapotranspiration from Relative Humidity at Equilibrium (ETRHEQ) method—that has been extensively evaluated against observations and shown to be empirically successful (Rigden & Salvucci, 2015; Salvucci & Gentine, 2013).

The results of earlier work (McColl et al., 2019), which were primarily about gaining theoretical insight, were focused exclusively on steady conditions. In the real world, the diurnal cycle ensures that steady conditions are never achieved. Is equation (1) accurate in real-world, unsteady conditions? In response to this question, in this study, we provide empirical and analytical evidence that equation (1) also applies reasonably well in transient, real-world conditions. Specifically, we evaluate equation (1) against global eddy covariance measurements of ET, showing that it performs well over a wide range of conditions. This is significant because it shows that water-limited B over inland continental regions can be estimated *solely* using atmospheric observations at daily to monthly time scales. Since equation (1) is simple and contains no free parameters, it demonstrates an emergent simplicity to continental ET that has not been previously recognized.

2. Methods

2.1. Surface Flux Equilibrium (SFE)

We briefly review the concept of "surface flux equilibrium" proposed in McColl et al. (2019). The near-surface atmospheric state (specifically, near-surface air temperature and specific humidity) is sensitive, to some degree, to turbulent surface fluxes (sensible heat flux and evapotranspiration, respectively). If this sensitivity is sufficiently strong, then higher atmospheric specific humidity is a signal of higher evapotranspiration in the recent past; similarly, higher temperature is a signal of higher sensible heat flux in the

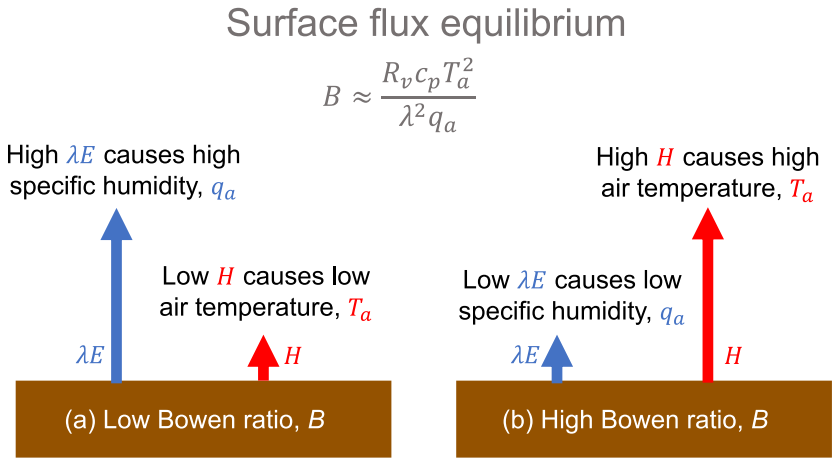

Figure 1. Surface flux equilibrium. In many continental regions, coupling between the land and atmosphere causes surface information, encoded in the Bowen ratio B, to become encoded in the near-surface atmospheric state on daily to monthly time scales. (a) A lower Bowen ratio B is associated with (i) reduced sensible heating (decreased H), leading to a cooler (decreased T_a) near-surface atmosphere, and (ii) increased ET (increased λE), leading to a wetter (increased q_a) near-surface atmosphere. (b) A higher B is associated with (i) increased H, leading to increased T_a, and (ii) decreased λE, leading to decreased q_a.

recent past. One consequence of strong sensitivity is that, to a good approximation, a balance exists between the surface moistening and surface heating terms in the near-surface relative humidity budget; this balance defines SFE (Figure 1 and supporting information Text S1). Furthermore, it leads directly to equation (1) and is exactly equivalent to a previous method (Rigden & Salvucci, 2015; Salvucci & Gentine, 2013) for estimating ET under steady conditions (Text S2). In this study, we test the hypothesis that SFE is a reasonable representation of real-world (i.e., transient) inland continental regions. Regions with substantial moisture or heat convergence (such as land regions near coasts) are not expected to be in SFE.

2.2. Data

Collocated measurements of half-hourly latent heat flux λE (W m^{-2}), sensible heat flux H (W m^{-2}), net radiation R_n (W m^{-2}), ground heat flux G (W m^{-2}), near-surface air temperature T_a (K), relative humidity r (-), wind speed u (m s^{-1}) and atmospheric pressure P (Pa) were obtained from the FLUXNET (fluxnet.ornl.gov) and AmeriFlux (ameriflux.lbl.gov) networks. For FLUXNET measurements, data with poor quality gap filling, as labeled in the quality control flags, were excluded. In addition, half-hourly measurements were excluded if the half-hourly surface energy imbalance was greater than 300 W m^{-2}, consistent with Rigden and Salvucci (2015).

Since surface flux equilibrium is hypothesized to apply to inland continental regions, we removed all sites within 250 km of the coast or a large water body. This filtering process resulted in 76 sites (Anthoni et al., 2004; Ardo et al., 2008; Barr & Black, 2018; Bergeron et al., 2007; Beringer et al., 2011; Bernhofer et al., 2016c; Bowling et al., 2010; Brunsell, 2016a, 2016b; 2016c; Cernusak et al., 2011; Chen et al., 2009; Cleverly et al., 2016, 2013; Cook & Coulter, 2016; Dong, 2016; Dore & Kolb, 2016a, 2016b, 2016c; Dragoni et al., 2011; Dušek et al., 2012; Ewers et al., 2016; Ewers & Pendall, 2016; Fischer et al., 2007; Flerchinger et al., 2019; Grünwald & Bernhofer, 2007; Hommeltenberg et al., 2014; Imer et al., 2013; Iwata et al., 2018; Kato et al., 2006; Knohl et al., 2003; Kueppers et al., 2018a, 2018b; Kurbatova et al., 2008; Lindauer et al., 2014; Liu & Randerson, 2008; Marchesini et al., 2007; Margolis, 2018, 2016; Merbold et al., 2014, 2009; Meyers, 2016a, 2016b, 2016c, 2016d, 2016e, 2016f, 2016g, 2018b, 2018a; Mkhabela et al., 2009; Monson et al., 2002; Moreo, 2018; Nakai et al., 2013; Prescher et al., 2010; Prober et al., 2012; Prueger & Parkin, 2016; Raz-Yaseef et al., 2015; Scott et al., 2015, 2010; Ulke et al., 2015; Verma et al., 2005; Wood & Gu, 2016; Yee et al., 2015; Zeller & Nikolov, 2000; Zona & Oechel, 2018), spanning a wide range of continents, climates, and biomes (Figure S1). Further details on each site—including its location and temporal record—are given in Tables S1 and S2.

At each site, measurements were aggregated to daily and monthly averages. Consistent with previous studies (Michel et al., 2016; Rigden & Salvucci, 2015; Salvucci & Gentine, 2013), we retained nighttime data in estimating daily and monthly averages (throughout this study, a "daily" average refers to an average over

a full 24-hr period, rather than just daylight hours). In estimating daily averages, days with any missing half-hourly data were excluded. Furthermore, days in which the daily surface energy imbalance was greater than 50 W m^{-2} were also excluded, consistent with Rigden and Salvucci (2015). In estimating monthly averages, months with fewer than 15 complete days of data were excluded.

2.3. Evaluation at All Sites

In addition to the direct measurements of λE provided by eddy covariance, the daily and monthly averaged observations at the 76 continental sites were used as inputs to calculate λE in four different ways: (i) the residual of the surface energy budget, (ii) the Priestley-Taylor equation (Priestley & Taylor, 1972), (iii) an Advection-Aridity equation based on the complementary relationship (Brutsaert & Stricker, 1979), and (iv) equation (1).

First, latent heat flux was calculated by solving for λE as the residual of the surface energy budget: $\lambda E = R_n - G - H$, using flux tower measurements of $R_n - G - H$. The difference between this estimate of latent heat flux and the direct measurement from eddy covariance data is a measure of the surface energy budget imbalance and the inherent uncertainty in the eddy covariance measurements.

Second, the Priestley-Taylor equation $\lambda E = \frac{\alpha\epsilon(R_n - G)}{\epsilon+1}$, where $\alpha = 1.26$ and $\epsilon = \frac{\lambda}{c_p}\frac{\mathrm{d}q^*}{\mathrm{d}T} = \frac{\lambda}{c_p}\frac{\lambda q^*(T_a)}{R_v T_a^2}$, was used similarly to calculate λE. The Priestley-Taylor equation provides an estimate of daytime ET over saturated surfaces.

Third, an Advection-Aridity equation from Brutsaert and Stricker (1979) (their equation (20)) was used to calculate latent heat flux. This equation requires wind speed as an additional input. The formulation used is based on the original wind function proposed by Penman (1948), as given in equation (18) of Brutsaert and Stricker (1979). We use the wind speed reported at each FLUXNET and AmeriFlux site, even though the (unreported) measurement height may deviate from the 2 m reference height for which the equation was originally designed.

Fourth, equation (1) was used to estimate B and converted to latent heat flux using the relation $\lambda E = \frac{R_n - G}{1+B}$.

We compare SFE to the Priestley-Taylor and Advection-Aridity equations because they are similar in not requiring calibration and in not requiring land surface information as inputs. The Priestley-Taylor equation does not require specific humidity as an input, meaning that it is simpler than SFE. The Advection-Aridity equation requires the same inputs as SFE, and also near-surface wind speed, meaning that it is more complicated than SFE. Various other forms of the complementary relationship exist, but many of these require land surface inputs (e.g., soil moisture or vegetation height). We further discuss differences between SFE and the complementary relationship in section 4.1.

The four different latent heat flux estimates were compared to the latent heat flux directly measured from eddy covariance at each site. The root-mean-square error (RMSE) and mean bias were calculated for all four estimates with respect to the directly measured latent heat flux. We choose the RMSE as a primary comparison metric of interest in this study because it is more appropriate for model selection: Since neither equation (1) nor the Priestley-Taylor equation nor the Advection-Aridity equation require any parameters to be fit to data, the Akaike information criterion (AIC) is a monotonic increasing function of RMSE. Therefore, comparing the models with respect to RMSE is equivalent to comparing them with respect to the AIC, a common approach to choosing between competing models.

2.4. Climatological Daily Mean Time Series at Focus Sites

Multiyear daily averaged data were further averaged over multiple years to create climatological daily mean time series of eddy covariance λE (both directly measured and calculated as the residual of the surface energy budget), and λE estimated using equation (1), the Priestley-Taylor equation, and the Advection-Aridity equation. The resulting time series were then smoothed using a 5-day moving average. We discarded sites in which there were missing values in any of the smoothed climatological daily mean λE time series. Twenty-eight sites met this criterion. Six of these sites, denoted "focus sites," were chosen as broadly representative and are presented in Figure 3. The sites span both Northern and Southern Hemispheres and include cropland (DE-Gri), savannas (SD-Dem and AU-ASM), deciduous broadleaf forest (ZM-Mon), and evergreen needleleaf forest (RU-Fyo and US-Fuf). Equivalent figures for the 22 other sites are shown in Figures S2–S5.

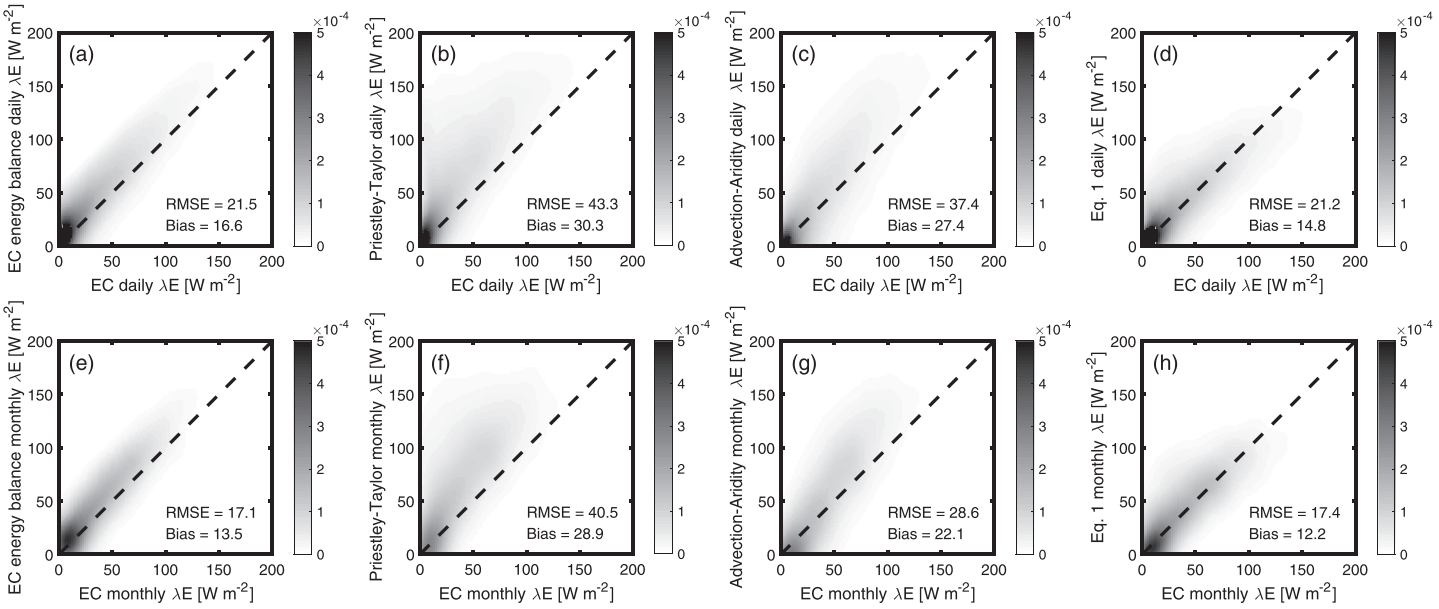

Figure 2. Comparison with eddy covariance measurements of daily (a–d) and monthly (e–h) λE (W m^{-2}), estimated using (a, e) the residual of the surface energy budget, (b, f) the Priestley-Taylor equation, (c, g) the Advection-Aridity equation, and (d, h) equation (1). RMSE is root-mean-square error (W m^{-2}). Shaded areas and color bars show the estimated joint empirical distribution functions of the variables listed on the horizontal and vertical axes of each plot. Dashed lines are 1:1 lines. The biases reported in (a) and (e) are exactly equal to the mean surface energy budget closure error in the eddy covariance data across sites at daily and monthly time scales, respectively.

The calculated errors in the eddy covariance measurements and in the SFE estimates at each of these 28 sites were compared with the annual mean evaporative fraction. The evaporative fraction is a ratio of noisy measurements, meaning it is particularly sensitive to measurement errors. To mitigate this problem, the annual mean evaporative fraction was calculated as the annual average of the ratio of monthly mean latent heat flux to monthly mean available energy.

3. Results

Figures 2d and 2h show that equation (1) is relatively accurate across a wide range of conditions, at both daily and monthly time scales. For comparison, we calculate λE as the residual of the surface energy budget components obtained from eddy covariance measurements and compare this estimate to the latent heat flux directly measured by eddy covariance (Figures 2a and 2e). If there were no errors in the eddy covariance measurements, there would be no difference between these two values; however, since there are well-known energy balance closure errors in eddy covariance measurements (Aubinet et al., 2012), the values differ. The errors in this comparison (Figures 2a and 2e) provide an approximate upper bound on the performance of any ET model when compared with eddy covariance measurements: Since the eddy covariance data are subject to errors of 10–30% themselves (Aubinet et al., 2012), even a model with perfect performance would exhibit errors of similar magnitude to those shown in Figures 2a and 2e when compared to eddy covariance measurements. In this light, the error statistics for equation (1) presented in Figures 2d and 2h are particularly impressive. The RMSE values also compare well to equivalent values from a recent intercomparison of substantially more complicated ET estimation algorithms, which reported values in the range 21–56 W m^{-2} based on daily eddy covariance measurements (Michel et al., 2016).

On the other hand, if errors in eddy covariance measurements are large enough, then even an extremely inaccurate ET model might yield comparable error statistics. To mitigate this concern, we also present equivalent plots, except replacing equation (1) with two alternative estimates of ET of comparable complexity: the Priestley-Taylor equation (Figures 2b and 2f) and the Advection-Aridity equation (Figures 2c and 2g). The Priestley-Taylor equation, which is used to estimate daytime ET over saturated surfaces, has substantially poorer error statistics compared to equation (1) and the eddy covariance measurements, as expected, since most land surfaces are not saturated. The Advection-Aridity equation, which is based on the complementary relationship (Bouchet, 1963; Brutsaert & Stricker, 1979; Morton, 1969), also has poorer error statistics than

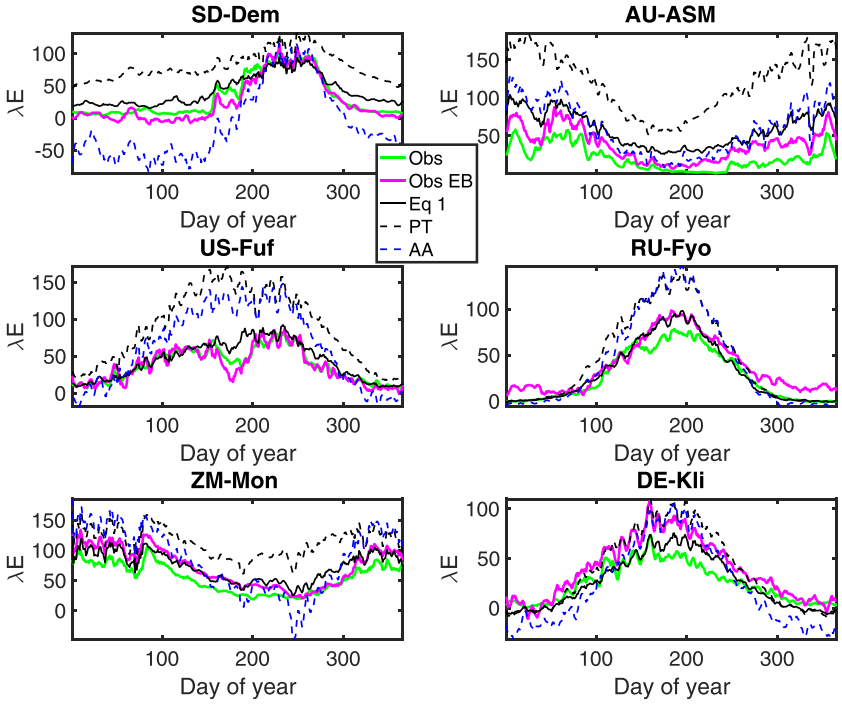

Figure 3. Climatological daily mean λE (W m^{-2}) time series at six focus sites. Site codes are listed in Tables S1 and S2. "Obs" is the latent heat flux directly measured from the eddy covariance data. "Obs EB" is the latent heat flux indirectly estimated (as the residual of the surface energy budget) from the eddy covariance data. "Eq 1" is the latent heat flux estimated using equation (1). "PT" is the latent heat flux estimated using the Priestley-Taylor equation (Priestley & Taylor, 1972). "AA" is the latent heat flux estimated using the Advection-Aridity equation (Brutsaert & Stricker, 1979).

both equation (1) and the eddy covariance measurements. This is surprising, since the Advection-Aridity equation requires wind speed as an additional input, beyond those required by SFE. The poorer performance may be due, in part, to the fact that the wind speed observations used in this study are not necessarily measured at a reference height of 2 m. If so, this demonstrates the sensitivity of the Advection-Aridity equation to a quantity that is often not reported and to the details of uncertain parameterizations of turbulence. These results demonstrate that the comparable error statistics between SFE and eddy covariance measurements are more than just a coincidence. Overall, our results demonstrate that equation (1) performs considerably better than comparable methods and even exhibits errors similar to those in eddy covariance measurements.

Figure 3 shows that equation (1) is also typically quite accurate at individual sites in inland continental regions. We highlight this performance at six focus sites. The focus sites are chosen to be hydrologically and climatologically diverse. They are also chosen to be broadly representative of the accuracy of equation (1), although there is considerable variability in accuracy between sites; equivalent plots for the full set of sites are presented in Figures S2–S5. Equation (1) broadly reproduces the observed climatology at each site, although it slightly overestimates ET under particularly dry conditions. Figure S8 shows that there is some weak structure to the errors in the SFE estimates: SFE errors are greatest at the driest sites, where annual mean evaporative fraction is particularly low.

Equation (1) outperforms the Priestley-Taylor and Advection-Aridity equations (in terms of errors estimated by comparing each method with λE directly measured using eddy covariance) at the vast majority of sites (Figure S6). Overall, compared to both the Priestley-Taylor and Advection-Aridity equations, it has both lower RMSE and mean bias at 93% of sites. Remarkably, it also has lower RMSE and mean bias compared with the estimated error in the eddy covariance measurements at a majority of sites (54% and 57% for RMSE and mean bias, respectively), even after substantially filtering the eddy covariance measurements to remove sites where energy balance closure errors are particularly high.

4. Discussion

4.1. Relation to Previous Work

It has been shown previously that, under steady conditions, equation (1) predicted by SFE is exactly equivalent to ETRHEQ (McColl et al., 2019). In Text S2, we extend this comparison to provide analytical arguments for why SFE and ETRHEQ remain similar under unsteady diurnally varying conditions. The derivation shows that under unsteady conditions, the right-hand side of equation (1) is multiplied by a random variable, which is constrained by air temperature and specific humidity. We characterize this random variable (denoted Λ) at all eddy covariance sites with sufficient observations, showing that its mean is very close to one—both at all sites individually and across all sites—with relatively little variability around this value (Figure S7). Therefore, SFE (equation (1)) is a reasonable approximation of ETRHEQ even under real-world, diurnally varying conditions (note that Λ is not a calibration parameter, since this analysis shows that setting $\Lambda = 1$ everywhere is reasonable). Since ETRHEQ has been extensively evaluated at a variety of temporal and spatial scales and shown to perform well (Rigden & Salvucci, 2015; Salvucci & Gentine, 2013), this lends further credibility to SFE, beyond our direct comparison with eddy covariance measurements in this study. The major advantages of SFE over ETRHEQ are that it does not require any land surface information (ETRHEQ requires vegetation height) or wind speed observations as inputs and avoids using uncertain semiempirical parameterizations of surface roughness and stratified turbulence. Furthermore, SFE consists of a single explicit equation, while ETRHEQ couples the energy balance and diffusion equations and needs to be solved using iterative methods.

Equation (1) is similar to, but distinct from, previous work on "equilibrium" ET, which predicts $B \approx \frac{R_v c_p T_a^2}{\lambda^2 q^*(T_a)}$ over idealized saturated surfaces (Raupach, 2001; Slatyer & McIlroy, 1961). In contrast to equilibrium estimates, SFE is accurate across a wide range of surface conditions, including substantially water-limited conditions (see McColl et al., 2019, for a detailed comparison between SFE and equilibrium ET).

SFE is also conceptually similar to the "complementary relationship" (Bouchet, 1963; Brutsaert & Stricker, 1979; Morton, 1969), which has been used to estimate ET from mostly meteorological data. In contrast to SFE, some implementations of the complementary relationship require a free parameter, which varies considerably between studies (Kahler & Brutsaert, 2006; Pettijohn & Salvucci, 2009). Mechanistic models of this parameter still require at least some land surface information, such as soil moisture (Aminzadeh et al., 2016). Other implementations of the complementary relationship, such as the Advection-Aridity equation (Brutsaert & Stricker, 1979) used in this study, do not require a free parameter. However, these implementations, when applied to daily time scales, still require observations of wind speed and, in many cases, vegetation height to parameterize turbulent transport. None of this is required by SFE.

Equation (1) predicts that, all else being equal, higher ET will be associated with higher relative humidity on daily to monthly time scales. Since drier atmospheres are known to promote more ET, this prediction might appear puzzling. In fact, both predictions are correct but apply to different time scales. Instantaneously, ET increases with increasing atmospheric dryness. However, over daily or longer time periods, ET moistens and cools the lower atmosphere, resulting in higher ET being associated with higher relative humidity (Betts, 2000; Novick et al., 2016; Zhou et al., 2019). Similarly, recent work has suggested that near-surface atmospheric humidity is largely set by the ocean and atmosphere, with the land surface playing a relatively passive role (Byrne & O'Gorman, 2016, 2018), a result that might appear to contradict SFE. However, that work applies to annual and longer time scales and global spatial scales, over which B will be substantially determined by atmospheric conditions. For example, while a wet surface with large ET will lead to a moist atmosphere at daily to monthly time scales, if anomalously high atmospheric drying persists long enough, the surface will dry out and eventually ET and near-surface humidity will reflect this. In this case, SFE still applies, but B is substantially determined by longer time scale processes, resulting in correlations with slower processes in the atmosphere and ocean. Furthermore, a recent study (Yin et al., 2019) providing a means for estimating the evaporative fraction (and, therefore, B) solely from atmospheric observations applies to multiyear time scales, rather than the daily to monthly time scales applicable to SFE.

4.2. Limitations

Equation (1) is substantially simpler than most methods for estimating ET, including the ETRHEQ method, but has comparable performance. This is particularly noteworthy, since it has zero parameters and exhibits good performance without tuning or calibration. Like ETRHEQ, SFE systematically overestimates ET when ET is very low and underestimates it when it is very high (Salvucci & Gentine, 2013). The positive bias at

low values may be due to the longer time required to achieve equilibrium when ET is small, reducing the likelihood that the system achieves equilibrium in the real world (McColl et al., 2019; Raupach, 2001). The negative bias at high values may be due to enhanced sensitivity to boundary layer drying by entrainment, advection, or cloud base mass flux, particularly under strongly convective conditions or at irrigated sites in otherwise dry regions. Strong sensitivity to these fluxes would violate the assumptions of SFE. Entrainment drying has been shown mechanistically to enhance ET over saturated surfaces on time scales of several hours as the boundary layer grows during the day (De Bruin, 1983; Raupach, 2000). However, its contribution to the full diel (i.e., 24 hr) cycle average, relevant to SFE, is likely smaller, given that entrainment is much smaller at night. In any case, most continental regions fall somewhere between the dry and saturated limiting cases where these biases occur.

Furthermore, like ETRHEQ, SFE is not expected to hold in coastal areas, where substantial atmospheric convergence dominates surface fluxes in setting the atmospheric state. It is also not clear that SFE will hold over oceans, since relative contributions to the near-surface diel-averaged state from radiation, surface fluxes, entrainment, and cloud base mass flux are fundamentally different compared with land surfaces; nor is it clear that SFE will hold in future climates as the world warms. Despite these caveats, our results demonstrate that SFE is sufficient to explain most of the observed signal in global eddy covariance measurements over inland continental regions, spanning a wide range of conditions, without calibration or tuning of parameters.

4.3. Future Applications

By drastically simplifying the representation of continental ET, equation (1) opens up considerable new opportunities for constraining terrestrial water, energy, and carbon budgets. First, since observations of air temperature and specific humidity have much greater spatial and temporal coverage compared to existing observations of B, SFE substantially increases available observations of continental evapotranspiration. Second, equation (1) provides a constraint on models that might prove useful in evaluating existing models and developing new models that faithfully represent land-atmosphere coupling. Third, it opens up a new opportunity for remote sensing of ET, using remotely sensed estimates of near-surface atmospheric temperature and specific humidity, which is substantially less model-based compared to existing methods.

Acknowledgments
Thanks to Guido Salvucci, Pierre Gentine, Russ Scott, and Michael Roderick for helpful discussions; to Qing He for preliminary data analyses; to Dan Chavas for his publicly available dist_from_coast Matlab code; and to the contributors to the FLUXNET (fluxnet.ornl.gov) and AmeriFlux (ameriflux.lbl.gov) databases. K. A. M. acknowledges funding from a Winokur Seed Grant in Environmental Sciences from Harvard University's Center for the Environment. A. J. R. acknowledges funding from The Rockefeller Foundation Planetary Health Fellows program at Harvard University. This work used eddy covariance data acquired and shared by the FLUXNET community, including these networks: AmeriFlux, AfriFlux, AsiaFlux, CarboAfrica, CarboEuropeIP, CarboItaly, CarboMont, ChinaFlux, Fluxnet-Canada, GreenGrass, ICOS, KoFlux, LBA, NECC, OzFlux-TERN, TCOS-Siberia, and USCCC. The ERA-Interim reanalysis data are provided by ECMWF and processed by LSCE. The FLUXNET eddy covariance data processing and harmonization was carried out by the European Fluxes Database Cluster, AmeriFlux Management Project, and Fluxdata project of FLUXNET, with the support of CDIAC and ICOS Ecosystem Thematic Center, and the OzFlux, ChinaFlux and AsiaFlux offices. Funding for AmeriFlux data resources was provided by the U.S. Department of Energy's Office of Science.

References

Aminzadeh, M., Roderick, M. L., & Or, D. (2016). A generalized complementary relationship between actual and potential evaporation defined by a reference surface temperature. *Water Resources Research*, *52*, 385–406. https://doi.org/10.1002/2015WR017969

Anderson, M. C., Kustas, W. P., Norman, J. M., Hain, C. R., Mecikalski, J. R., Schultz, L., et al. (2011). Mapping daily evapotranspiration at field to continental scales using geostationary and polar orbiting satellite imagery. *Hydrology and Earth System Sciences*, *15*(1), 223–239.

Anthoni, P. M., Knohl, A., Rebmann, C., Freibauer, A., Mund, M., Ziegler, W., et al. (2004). Forest and agricultural land-use-dependent CO_2 exchange in Thuringia, Germany. *Global Change Biology*, *10*(12), 2005–2019. https://doi.org/10.1111/j.1365-2486.2004.00863.x

Ardo, J., Molder, M., El-Tahir, B. A., & Elkhidir, H. A. M. (2008). Seasonal variation of carbon fluxes in a sparse savanna in semi arid Sudan. *Carbon Balance and Management*, *3*(1), 7. https://doi.org/10.1186/1750-0680-3-7

Aubinet, M., Vesala, T., & Papale, D. (Eds.) (2012). *Eddy covariance Edited by* Aubinet, M., Vesala, T., & Papale, D. Dordrecht: Springer Netherlands.

Ball, J. T., Woodrow, I. E., & Berry, J. A. (1987). A model predicting stomatal conductance and its contribution to the control of photosynthesis under different environmental conditions. In J. Biggins (Ed.), *Progress in photosynthesis research: Volume 4 Proceedings of the VIIth International Congress on Photosynthesis Providence, Rhode Island, USA, August 10–15, 1986* (pp. 221–224). Dordrecht: Springer Netherlandsen. https://doi.org/10.1007/978-94-017-0519-6-48

Barr, A., & Black, A. T. (2018). Ameriflux CA-SJ2 Saskatchewan—Western boreal, jack pine forest harvested in 2002 from 2003–present. https://doi.org/10.17190/AMF/1436321

Bastiaanssen, W. G. M., Menenti, M., Feddes, R. A., & Holtslag, A. A. M. (1998). A remote sensing surface energy balance algorithm for land (SEBAL). 1. Formulation. *Journal of Hydrology*, *212-213*, 198–212.

Bergeron, O., Margolis, H. A., Black, T. A., Coursolle, C., Dunn, A. L., Barr, A. G., & Wofsy, S. C. (2007). Comparison of carbon dioxide fluxes over three boreal black spruce forests in Canada. *Global Change Biology*, *13*(1), 89–107. https://doi.org/10.1111/j.1365-2486.2006.01281.x

Beringer, J., Hutley, L. B., Hacker, J. M., Neininger, B., & U, K. T. P. (2011). Patterns and processes of carbon, water and energy cycles across northern Australian landscapes: From point to region. *Agricultural and Forest Meteorology*, *151*(11), 1409–1416. https://doi.org/10.1016/j.agrformet.2011.05.003

Bernhofer, C., Grunwald, T., Moderow, U., Hehn, M., Eichelmann, U., & Prasse, H. (2016). Fluxnet2015 de-obe oberbarenburg from 2008–2014. https://doi.org/10.18140/FLX/1440151

Betts, A. K. (2000). Idealized model for equilibrium boundary layer over land. *Journal of Hydrometeorology*, *1*(6), 507–523.

Bouchet, R. J. (1963). Evapotranspiration reelle, evapotranspiration potentielle, et production agricole. *Annales Agronomiques*, *14*, 743–824.

Bowling, D. R., Bethers-Marchetti, S., Lunch, C. K., Grote, E. E., & Belnap, J. (2010). Carbon, water, and energy fluxes in a semiarid cold desert grassland during and following multiyear drought. *Journal of Geophysical Research*, *115*, G04026. https://doi.org/10.1029/2010JG001322

Brondani, D. V., Acevedo, O. C., Tatsch, J. D., & Puhales, F. S. (2019). Estimating monthly energy fluxes using observations of near-surface air temperature, humidity and radiosonde profiles. *Boundary-Layer Meteorology*, *171*(2), 271–288. https://doi.org/10.1007/s10546-019-00429-4

Brunsell, N. (2016a). Ameriflux US-KFS Kansas field station from 2007–present. https://doi.org/10.17190/AMF/1246132

Brunsell, N. (2016b). AmeriFlux US-KLS Kansas Land Institute from 2012-. https://doi.org/10.17190/AMF/1498745

Brunsell, N. (2016c). Ameriflux US-KON Konza prairie lter (knz) from 2006–present. https://doi.org/10.17190/AMF/1246068

Brutsaert, W., & Stricker, H. (1979). An advection-aridity approach to estimate actual regional evapotranspiration. *Water Resources Research*, *15*(2), 443–450. https://doi.org/10.1029/WR015i002p00443

Byrne, M. P., & O'Gorman, P. A. (2016). Understanding decreases in land relative humidity with global warming: Conceptual model and GCM simulations. *Journal of Climate*, *29*(24), 9045–9061. https://doi.org/10.1175/JCLI-D-16-0351.1

Byrne, M. P., & O'Gorman, P. A. (2018). Trends in continental temperature and humidity directly linked to ocean warming. *Proceedings of the National Academy of Sciences*, *115*, 4863–4868. https://doi.org/10.1073/pnas.1722312115

Cernusak, L. A., Hutley, L. B., Beringer, J., Holtum, J. A. M., & Turner, B. L. (2011). Photosynthetic physiology of eucalypts along a sub-continental rainfall gradient in northern Australia. *Agricultural and Forest Meteorology*, *151*(11), 1462–1470.

Chen, S., Chen, J., Lin, G., Zhang, W., Miao, H., Wei, L., et al. (2009). Energy balance and partition in Inner Mongolia steppe ecosystems with different land use types. *Agricultural and Forest Meteorology*, *149*(11), 1800–1809.

Cleverly, J., Boulain, N., Villalobos-Vega, R., Grant, N., Faux, R., Wood, C., et al. (2013). Dynamics of component carbon fluxes in a semi-arid acacia woodland, central Australia. *Journal of Geophysical Research: Biogeosciences*, *118*, 1168–1185. https://doi.org/10.1002/jgrg.20101

Cleverly, J., Eamus, D., Van Gorsel, E., Chen, C., Rumman, R., Luo, Q., et al. (2016). Productivity and evapotranspiration of two contrasting semiarid ecosystems following the 2011 global carbon land sink anomaly. *Agricultural and Forest Meteorology*, *220*, 151–159.

Cook, D., & Coulter, R. L. (2016). Ameriflux US-WLR Walnut River watershed (Smileyburg) from 2001–2004. https://doi.org/10.17190/AMF/1246115

De Bruin, H. A. R. (1983). A model for the Priestley-Taylor parameter. *Journal of Climate and Applied Meteorology*, *22*(4), 572–578.

Dong, G. (2016). Fluxnet2015 CN-CNG changling from 2007–2010. https://doi.org/10.18140/FLX/1440209

Dore, S., & Kolb, T. (2016a). Ameriflux US-FMF Flagstaff—Managed forest from 2006–2010. https://doi.org/10.17190/AMF/1246050

Dore, S., & Kolb, T. (2016b). Ameriflux US-FUF Flagstaff—Unmanaged forest from 2006–2010. https://doi.org/10.17190/AMF/1246051

Dore, S., & Kolb, T. (2016c). Ameriflux US-FWF Flagstaff—Wildfire from 2006–2010. https://doi.org/10.17190/AMF/1246052

Dragoni, D., Schmid, H. P., Wayson, C. A., Potter, H., Grimmond, C. S. B., & Randolph, J. C. (2011). Evidence of increased net ecosystem productivity associated with a longer vegetated season in a deciduous forest in south-central Indiana, USA. *Global Change Biology*, *17*(2), 886–897.

Dušek, J., Čížková, H., Stellner, S., Czerný, R., & Květ, J. (2012). Fluctuating water table affects gross ecosystem production and gross radiation use efficiency in a sedge-grass marsh. *Hydrobiologia*, *692*(1), 57–66.

Ewers, B., & Pendall, E. (2016). Ameriflux US-WDN Walden from 2006–2008. https://doi.org/10.17190/AMF/1246832

Ewers, B., Pendall, E., & Reed, D. (2016). Ameriflux US-CPK Chimney Park from 2009–present. https://doi.org/10.17190/AMF/1246150

Farquhar, G. D., von Caemmerer, S., & Berry, J. A. (1980). A biochemical model of photosynthetic CO_2 assimilation in leaves of C3 species. *Planta*, *149*(1), 78–90.

Fischer, M. L., Billesbach, D. P., Berry, J. A., Riley, W. J., & Torn, M. S. (2007). Spatiotemporal variations in growing season exchanges of CO_2, H_2O, and sensible heat in agricultural fields of the Southern Great Plains. *Earth Interactions*, *11*(17), 1–21.

Fisher, J. B., Tu, K. P., & Baldocchi, D. D. (2008). Global estimates of the land–atmosphere water flux based on monthly AVHRR and ISLSCP-II data, validated at 16 FLUXNET sites. *Remote Sensing of Environment*, *112*(3), 901–919.

Flerchinger, G. N., Fellows, A. W., Seyfried, M. S., Clark, P. E., & Lohse, K. A. (2019). Water and carbon fluxes along an elevational gradient in a sagebrush ecosystem. *Ecosystems*, 1–18. https://doi.org/10.1007/s10021-019-00400-x

Friedlingstein, P., Meinshausen, M., Arora, V. K., Jones, C. D., Anav, A., Liddicoat, S. K., & Knutti, R. (2013). Uncertainties in CMIP5 climate projections due to carbon cycle feedbacks. *Journal of Climate*, *27*(2), 511–526.

Gentine, P., Chhang, A., Rigden, A., & Salvucci, G. (2016). Evaporation estimates using weather station data and boundary layer theory. *Geophysical Research Letters*, *43*, 11,661–11,670. https://doi.org/10.1002/2016GL070819

Gentine, P., Ferguson, C. R., & Holtslag, A. A. M. (2013). Diagnosing evaporative fraction over land from boundary-layer clouds. *Journal of Geophysical Research: Atmospheres*, *118*, 8185–8196. https://doi.org/10.1002/jgrd.50416

Green, J. K., Seneviratne, S. I., Berg, A. M., Findell, K. L., Hagemann, S., Lawrence, D. M., & Gentine, P. (2019). Large influence of soil moisture on long-term terrestrial carbon uptake. *Nature*, *565*(7740), 476.

Grünwald, T., & Bernhofer, C. (2007). A decade of carbon, water and energy flux measurements of an old spruce forest at the Anchor Station Tharandt. *Tellus B*, *59*(3), 387–396.

Hommeltenberg, J., Schmid, H. P., Drösler, M., & Werle, P. (2014). Can a bog drained for forestry be a stronger carbon sink than a natural bog forest? *Biogeosciences*, *11*(13), 3477–3493.

Imer, D., Merbold, L., Eugster, W., & Buchmann, N. (2013). Temporal and spatial variations of soil CO2, CH4 and N2O fluxes at three differently managed grasslands. *Biogeosciences*, *10*(9), 5931–5945.

Iwata, H., Ueyama, M., & Harazono, Y. (2018). Ameriflux US-UAF University of Alaska, Fairbanks from 2002–present. https://doi.org/10.17190/AMF/1480322

Kahler, D. M., & Brutsaert, W. (2006). Complementary relationship between daily evaporation in the environment and pan evaporation. *Water Resources Research*, *42*, W05413. https://doi.org/10.1029/2005WR004541

Kato, T., Tang, Y., Gu, S., Hirota, M., Du, M., Li, Y., & Zhao, X. (2006). Temperature and biomass influences on interannual changes in CO_2 exchange in an alpine meadow on the Qinghai-Tibetan Plateau. *Global Change Biology*, *12*(7), 1285–1298.

Knohl, A., Schulze, E.-D., Kolle, O., & Buchmann, N. (2003). Large carbon uptake by an unmanaged 250-year-old deciduous forest in central Germany. *Agricultural and Forest Meteorology*, *118*(3-4), 151–167.

Kueppers, L., Torn, M., & Biraud, S. (2018a). Ameriflux US-A32 ARM-SGP Medford hay pasture from 2015–present. https://doi.org/10.17190/AMF/1436327

Kueppers, L., Torn, M., & Biraud, S. (2018b). Ameriflux US-A74 ARM SGP Milo field from 2016–present. https://doi.org/10.17190/AMF/1436328

Kurbatova, J., Li, C., Varlagin, A., Xiao, X., & Vygodskaya, N. (2008). Modeling carbon dynamics in two adjacent spruce forests with different soil conditions in Russia. *Biogeosciences*, *5*(4), 969–980.

Lindauer, M., Schmid, H. P., Grote, R., Mauder, M., Steinbrecher, R., & Wolpert, B. (2014). Net ecosystem exchange over a non-cleared wind-throw-disturbed upland spruce forest—Measurements and simulations. *Agricultural and Forest Meteorology*, *197*, 219–234.

Liu, H., & Randerson, J. T. (2008). Interannual variability of surface energy exchange depends on stand age in a boreal forest fire chronosequence. *Journal of Geophysical Research*, *113*, G01006. https://doi.org/10.1029/2007JG000483
Ma, H.-Y., Klein, S. A., Xie, S., Zhang, C., Tang, S., Tang, Q., et al. (2018). CAUSES: On the role of surface energy budget errors to the warm surface air temperature error over the central United States. *Journal of Geophysical Research: Atmospheres*, *123*, 2888–2909. https://doi.org/10.1002/2017JD027194
Marchesini, L. B., Papale, D., Reichstein, M., Vuichard, N., Tchebakova, N., & Valentini, R. (2007). Carbon balance assessment of a natural steppe of southern Siberia by multiple constraint approach. *Biogeosciences Discussions*, *4*(1), 165–208. https://doi.org/10.5194/bgd-4-165-2007
Margolis, H. A. (2016). Ameriflux CA-QCU Quebec—Eastern boreal, black spruce/jack pine cutover from 2001–present. https://doi.org/10.17190/AMF/1246828
Margolis, H. (2018). Ameriflux CA-QC2 Quebec—1975 harvested black spruce (hbs75) from 2007–present. https://doi.org/10.17190/AMF/1419514
McColl, K. A., Salvucci, G. D., & Gentine, P. (2019). Surface flux equilibrium theory explains an empirical estimate of water-limited daily evapotranspiration. *Journal of Advances in Modeling Earth Systems*, *11*, 2036–2049. https://doi.org/10.1029/2019MS001685
Merbold, L., Ardö, J., Arneth, A., Scholes, R. J., Nouvellon, Y., de Grandcourt, A., et al. (2009). Precipitation as driver of carbon fluxes in 11 African ecosystems. *Biogeosciences*, *6*(6), 1027–1041.
Merbold, L., Eugster, W., Stieger, J., Zahniser, M., Nelson, D., & Buchmann, N. (2014). Greenhouse gas budget (CO_2, CH_4 and N_2O) of intensively managed grassland following restoration. *Global Change Biology*, *20*(6), 1913–1928.
Meyers, T. (2016a). Ameriflux US-BKG Brookings from 2004–present. https://doi.org/10.17190/AMF/1246040
Meyers, T. (2016b). Ameriflux US-BLK Black Hills from 2003–2008. https://doi.org/10.17190/AMF/1246031
Meyers, T. (2016c). Ameriflux US-CHR Chestnut Ridge from 2005–present. https://doi.org/10.17190/AMF/1246044
Meyers, T. (2016d). Ameriflux US-CTN Cottonwood from 2007–2009. https://doi.org/10.17190/AMF/1246117
Meyers, T. (2016e). Ameriflux US-FPE Fort Peck from 2000–present. https://doi.org/10.17190/AMF/1246053
Meyers, T. (2016f). Ameriflux US-SFP Sioux Falls portable from 2007–present. https://doi.org/10.17190/AMF/1246126
Meyers, T. (2016g). Ameriflux US-WBW Walker branch watershed from 1995–1999. https://doi.org/10.17190/AMF/1246109
Meyers, T. (2018a). Ameriflux US-GOO Goodwin Creek from 2002–2006. https://doi.org/10.17190/AMF/1246058
Meyers, T. (2018b). Ameriflux US-LWW Little Washita watershed from 1997–1998. https://doi.org/10.17190/AMF/1246073
Michel, D., Jimnez, C., Miralles, D. G., Jung, M., Hirschi, M., Ershadi, A., et al. (2016). The WACMOS-ET project—Partă1: Tower-scale evaluation of four remote-sensing-based evapotranspiration algorithms. *Hydrology and Earth System Sciences*, *20*(2), 803–822.
Miralles, D. G., Holmes, T. R. H., Jeu, R. A. M. De, Gash, J. H., Meesters, A. G. C. A., & Dolman, A. J. (2011). Global land-surface evaporation estimated from satellite-based observations. *Hydrology and Earth System Sciences*, *15*(2), 453–469.
Mkhabela, M. S., Amiro, B. D., Barr, A. G., Black, T. A., Hawthorne, I., Kidston, J., et al. (2009). Comparison of carbon dynamics and water use efficiency following fire and harvesting in Canadian boreal forests. *Agricultural and Forest Meteorology*, *149*(5), 783–794.
Monson, R. K., Turnipseed, A. A., Sparks, J. P., Harley, P. C., Scott-Denton, L. E., Sparks, K., & Huxman, T. E. (2002). Carbon sequestration in a high-elevation, subalpine forest. *Global Change Biology*, *8*(5), 459–478.
Monteith, J. L. (1965). Evaporation and environment. In G. E. Fogg (Ed.), *The state and movement of water in living organisms* (pp. 205–234). Cambridge, UK: Cambridge University Press.
Moreo, M. (2018). Ameriflux US-ADR Amargosa desert research site (ADRS) from 2011–present. https://doi.org/10.17190/AMF/1418680
Morton, F. I. (1969). Potential evaporation as a manifestation of regional evaporation. *Water Resources Research*, *5*(6), 1244–1255.
Mu, Q., Zhao, M., & Running, S. W. (2011). Improvements to a MODIS global terrestrial evapotranspiration algorithm. *Remote Sensing of Environment*, *115*(8), 1781–1800.
Mueller, B., & Seneviratne, S. I. (2014). Systematic land climate and evapotranspiration biases in CMIP5 simulations. *Geophysical Research Letters*, *41*, 128–134. https://doi.org/10.1002/2013GL058055
Nakai, T., Kim, Y., Busey, R. C., Suzuki, R., Nagai, S., Kobayashi, H., et al. (2013). Characteristics of evapotranspiration from a permafrost black spruce forest in interior Alaska. *Polar Science*, *7*(2), 136–148. https://doi.org/10.1016/j.polar.2013.03.003
Novick, K. A., Ficklin, D. L., Stoy, P. C., Williams, C. A., Bohrer, G., Oishi, A. C., et al. (2016). The increasing importance of atmospheric demand for ecosystem water and carbon fluxes. *Nature Climate Change*, *6*(11), 1023–1027.
Penman, H. L. (1948). Natural evaporation from open water, bare soil and grass. *Proceedings of the Royal Society of London. Series A. Mathematical and Physical Sciences*, *193*(1032), 120–145.
Pettijohn, J. C., & Salvucci, G. D. (2009). A new two-dimensional physical basis for the complementary relation between terrestrial and pan evaporation. *Journal of Hydrometeorology*, *10*(2), 565–574.
Prescher, A.-K., Grünwald, T., & Bernhofer, C. (2010). Land use regulates carbon budgets in eastern Germany: From NEE to NBP. *Agricultural and Forest Meteorology*, *150*(7-8), 1016–1025.
Priestley, C. H. B., & Taylor, R. J. (1972). On the assessment of surface heat flux and evaporation using large-scale parameters. *Monthly Weather Review*, *100*(2), 81–92.
Prober, S. M., Thiele, K. R., Rundel, P. W., Yates, C. J., Berry, S. L., Byrne, M., et al. (2012). Facilitating adaptation of biodiversity to climate change: A conceptual framework applied to the world's largest Mediterranean-climate woodland. *Climatic Change*, *110*(1-2), 227–248.
Prueger, J., & Parkin, T. (2016). Ameriflux US-BR1 Brooks field site 10- Ames from 2001–present. https://doi.org/10.17190/AMF/1246038
Raupach, M. R. (2000). Equilibrium evaporation and the convective boundary layer. *Boundary-Layer Meteorology*, *96*(1-2), 107–142.
Raupach, M. R. (2001). Combination theory and equilibrium evaporation. *Quarterly Journal of the Royal Meteorological Society*, *127*(574), 1149–1181.
Raz-Yaseef, N., Billesbach, D. P., Fischer, M. L., Biraud, S. C., Gunter, S. A., Bradford, J. A., & Torn, M. S. (2015). Vulnerability of crops and native grasses to summer drying in the U.S. Southern Great Plains. *Agriculture, Ecosystems & Environment*, *213*, 209–218. https://doi.org/10.1016/j.agee.2015.07.021
Rigden, A., Li, D., & Salvucci, G. (2018). Dependence of thermal roughness length on friction velocity across land cover types: A synthesis analysis using AmeriFlux data. *Agricultural and Forest Meteorology*, *249*, 512–519.
Rigden, A. J., & Salvucci, G. D. (2015). Evapotranspiration based on equilibrated relative humidity (ETRHEQ): Evaluation over the continental U.S. *Water Resources Research*, *51*, 2951–2973. https://doi.org/10.1002/2014WR016072
Salvucci, G. D., & Gentine, P. (2013). Emergent relation between surface vapor conductance and relative humidity profiles yields evaporation rates from weather data. *Proceedings of the National Academy of Sciences*, *110*(16), 6287–6291.
Scott, R. L., Biederman, J. A., Hamerlynck, E. P., & Barron-Gafford, G. A. (2015). The carbon balance pivot point of southwestern U.S. semiarid ecosystems: Insights from the 21st century drought. *Journal of Geophysical Research: Biogeosciences*, *120*, 2612–2624. https://doi.org/10.1002/2015jg003181

Scott, R. L., Hamerlynck, E. P., Jenerette, G. D., Moran, M. S., & Barron-Gafford, G. A. (2010). Carbon dioxide exchange in a semidesert grassland through drought-induced vegetation change. *Journal of Geophysical Research*, *115*, G03026. https://doi.org/10.1029/2010jg001348

Sellers, P. J., Dickinson, R. E., Randall, D. A., Betts, A. K., Hall, F. G., Berry, J. A., et al. (1997). Modeling the exchanges of energy, water, and carbon between continents and the atmosphere. *Science*, *275*(5299), 502–509.

Slatyer, R. O., & McIlroy, I. C. (1961). *Practical microclimatology: With special reference to the water factor in soil-plant-atmosphere relationships*. Melbourne, Australia: Commonwealth Scientific and Industrial Research Organisation.

Trugman, A. T., Medvigy, D., Mankin, J. S., & Anderegg, W. R. L. (2018). Soil moisture stress as a major driver of carbon cycle uncertainty. *Geophysical Research Letters*, *45*, 6495–6503. https://doi.org/10.1029/2018GL078131

Ulke, A. G., Gattinoni, N. N., & Posse, G. (2015). Analysis and modelling of turbulent fluxes in two different ecosystems in Argentina. *International Journal of Environment and Pollution*, *58*(1/2), 52. https://doi.org/10.1504/ijep.2015.076583

Verma, S. B., Dobermann, A., Cassman, K. G., Walters, D. T., Knops, J. M., Arkebauer, T. J., et al. (2005). Annual carbon dioxide exchange in irrigated and rainfed maize-based agroecosystems. *Agricultural and Forest Meteorology*, *131*(1-2), 77–96. https://doi.org/10.1016/j.agrformet.2005.05.003

Wood, J., & Gu, L. (2016). Ameriflux US-MOZ Missouri Ozark site from 2004–present. https://doi.org/10.17190/AMF/1246081

Yee, M. S., Pauwels, V. R. N., Daly, E., Beringer, J., Rüdiger, C., McCabe, M. F., & Walker, J. P. (2015). A comparison of optical and microwave scintillometers with eddy covariance derived surface heat fluxes. *Agricultural and Forest Meteorology*, *213*, 226–239. https://doi.org/10.1016/j.agrformet.2015.07.004

Yin, J., Calabrese, S., Daly, E., & Porporato, A. (2019). The energy side of Budyko: Surface-energy partitioning from hydrological observations. *Geophysical Research Letters*, *46*, 7456–7463. https://doi.org/10.1029/2019GL083373

Zeller, K. F., & Nikolov, N. T. (2000). Quantifying simultaneous fluxes of ozone, carbon dioxide and water vapor above a subalpine forest ecosystem. *Environmental Pollution*, *107*(1), 1–20.

Zhou, S., Zhang, Y., Williams, A. P., & Gentine, P. (2019). Projected increases in intensity, frequency, and terrestrial carbon costs of compound drought and aridity events. *Science Advances*, *5*(1), eaau5740.

Zona, D., & Oechel, W. (2018). Ameriflux US-IVO Ivotuk from 2003–present. https://doi.org/10.17190/AMF/1246067

Supporting Information for "Emergent simplicity of continental evapotranspiration"

Kaighin A. McColl[1,2] **and Angela J. Rigden**[1]

[1]Department of Earth and Planetary Sciences, Harvard University, Cambridge, MA 02138
[2]School of Engineering and Applied Sciences, Harvard University, Cambridge, MA 02138

Contents

Introduction

This document contains supporting text, figures and tables.

Text S1: Surface flux equilibrium theory

In this section, we review the theory of surface flux equilibrium presented in *McColl et al.* [2019]. For an atmospheric control volume touching the land surface at its lower boundary, with depth h [m], the specific humidity budget is

$$\frac{\partial q_a}{\partial t} = \frac{E}{\rho h} - F_q^h + C_q \tag{S1}$$

where q_a is the vertically-averaged specific humidity [-], E is evapotranspiration [kg m^2 s^{-1}], ρ is air density [kg m^{-3}], F_q^h is the vertical moisture flux out of the top of the control volume [s^{-1}], and C_q is vertically-averaged lateral moisture convergence [s^{-1}]. Sublimation is neglected. The potential temperature budget is

$$\frac{\partial \theta}{\partial t} = \frac{H}{\rho c_p h} - F_\theta^h + C_\theta - Q \tag{S2}$$

where θ is the vertically-averaged potential temperature [K], H is surface sensible heat flux [W m^{-2}], c_p is specific heat capacity of air at constant pressure [J kg^{-1} K^{-1}], F_θ^h is the vertical potential temperature flux out of the top of the control volume [K s^{-1}], C_θ is vertically-averaged lateral potential temperature convergence [K s^{-1}], and $-Q$ is vertically-averaged radiative cooling [K s^{-1}].

At screen-level (typically, about 2 m above the land surface), the potential temperature is equivalent to the actual air temperature ($\theta = T_a$), meaning the relative humidity can be written as $r = q_a/q^*(\theta)$. The relative humidity budget at screen-level is

Corresponding author: K.A. McColl, kmccoll@seas.harvard.edu

$$\frac{\partial r}{\partial t} = \frac{\partial r}{\partial q_a}\frac{\partial q_a}{\partial t} + \frac{\partial r}{\partial \theta}\frac{\partial \theta}{\partial t}$$
$$= \frac{1}{q^*(T_a)}\left(\overbrace{\frac{\lambda E}{\rho \lambda h}}^{\text{I: surface moistening}} - \overbrace{\frac{r\Delta H}{\rho c_p h}}^{\text{II: surface heating}} \right.$$
$$\left. + \underbrace{C_q - F_q^h}_{\text{III: atmospheric moistening}} - \underbrace{r\Delta(C_\theta - F_\theta^h - Q)}_{\text{IV: atmospheric heating}} \right) \tag{S3}$$

where $\Delta = \left.\frac{dq^*}{dT}\right|_{T=T_a} = \frac{\lambda}{c_p}\frac{\lambda q^*(T_a)}{R_v T_a^2}$. The theory of 'surface flux equilibrium' [*McColl et al.*, 2019] hypothesizes that the surface moistening and surface heating terms (terms I and II, respectively, in equation S3) approximately balance at daily to monthly time scales. The balance can be rewritten as

$$B \approx \frac{R_v c_p T_a^2}{\lambda^2 q_a} \tag{S4}$$

where $B = \frac{H}{\lambda E}$ is the Bowen ratio and $\epsilon \equiv \frac{\lambda\Delta}{c_p} = \frac{\lambda}{c_p}\left.\frac{dq^*}{dT}\right|_{T=T_a} = \frac{\lambda}{c_p}\frac{\lambda q^*(T_a)}{R_v T_a^2}$, where $\lambda = 2.5008 \times 10^6$ [J kg^{-1}] is the latent heat of vaporization of water, $c_p = 1005$ [J kg^{-1} K^{-1}] is the specific heat capacity of air at constant pressure and $R_v = 461.5$ [J kg^{-1} K^{-1}] is the gas constant for water vapor. The balance is caused by coupling between the land and atmosphere: decreasing the Bowen ratio ($B = \frac{H}{\lambda E}$) both reduces sensible heating and increases ET, resulting in a cooler (lower T_a), moister (higher q_a) near-surface atmosphere.

Text S2: Simplification of ETRHEQ under steady and transient conditions

One of the arguments provided in *McColl et al.* [2019] for the validity of SFE is that it is closely related to another approach for estimating ET, which has been carefully validated across a wide range of conditions [*Salvucci and Gentine*, 2013; *Rigden and Salvucci*, 2015]. In this section, we review a derivation provided in *McColl et al.* [2019] which showed that ETRHEQ and SFE are equivalent under steady (i.e., time-invariant) conditions. Furthermore, we extend the work of *McColl et al.* [2019] to derive a relation showing that ETRHEQ and SFE are very similar under diurnally-varying conditions.

Governing equations

The governing equations include the surface energy balance

$$R_n - G = H + \lambda E \tag{S5}$$

where the available energy $R_n - G$ is treated as an externally imposed, constant parameter. The turbulent fluxes are given by

$$H = \rho c_p g_a (T_s - \theta), \tag{S6}$$
$$\lambda E = \rho\lambda \frac{g_a g_s}{g_a + g_s}(q^*(T_s) - q_a) = \rho\lambda g_s (q^*(T_s) - q_s), \tag{S7}$$

where H is the sensible heat flux, ρ is air density, c_p is the specific heat capacity of air, g_a is atmospheric conductance, T_s is surface temperature, θ is the potential temperature

of the mixed layer, E is evaporation, λ is the latent heat of vaporization, g_s is the surface conductance, $q^*(T)$ is the saturation specific humidity at temperature T, q_a is the specific humidity of the mixed layer and q_s is specific humidity at the surface.

Linearizing $q^*(T_s)$ around $T_s = \theta$ gives

$$q^*(T_s) \approx q^*(\theta) + \Delta(T_s - \theta) \tag{S8}$$

where $\Delta = \left.\frac{dq^*}{dT}\right|_\theta$. Combining equations S5, S6, S7, and S8 gives the Penman-Monteith equation

$$\lambda E = \frac{\Delta(R_n - G) + \rho c_p g_a (q^*(\theta) - q_a)}{\Delta + \gamma(1 + \frac{g_a}{g_s})} \tag{S9}$$

which can be rearranged to give an expression for g_s:

$$\hat{g}_s = \frac{g_a \gamma \lambda E}{\Delta(R_n - G) - (\Delta + \gamma)\lambda E + g_a c_p (q^*(\theta) - q_a)} \tag{S10}$$

or equivalently

$$\hat{g}_s = \frac{g_a (R_n - G - H)}{g_a \lambda \rho (q^*(\theta) - q_a) - (R_n - G - (1 + \frac{\Delta}{\gamma})H)} \tag{S11}$$

where $\gamma = \frac{c_p}{\lambda}$.

Rearranging equation S7 gives

$$q_s = \frac{g_a q_a + g_s q^*(T_s)}{g_a + g_s} \tag{S12}$$

Dividing through by $q^*(T_s)$ gives

$$r_s = \frac{r\frac{q^*(\theta)}{q^*(T_s)} + \frac{g_s}{g_a}}{1 + \frac{g_s}{g_a}} \tag{S13}$$

Applying equations S8, S6, S5 and S9 gives

$$r_s = \frac{r\frac{q^*(\theta)}{R_n - G - \frac{\Delta(R_n - G) + \rho c_p g_a (q^*(\theta) - q_a)}{\Delta + \gamma(1 + \frac{g_a}{g_s})}} + \frac{g_s}{g_a}}{\frac{q^*(\theta) + \Delta \frac{\Delta(R_n - G) + \rho c_p g_a (q^*(\theta) - q_a)}{\Delta + \gamma(1 + \frac{g_a}{g_s})}}{\rho c_p g_a}} \tag{S14}$$

ETRHEQ [*Salvucci and Gentine*, 2013; *Rigden and Salvucci*, 2015] hypothesizes that the true value of g_s (defined here as $\hat{g}_s$) satisfies the condition

$$\frac{\partial}{\partial g_s}\left[\frac{1}{T}\int_0^T (r_s(t, g_s) - r(t))^2 dt\right]\Bigg|_{\hat{g}_s} = 0 \tag{S15}$$

We consider the steady-state and transient cases separately.

Steady-state case

In this section, we review the derivation provided in *McColl et al.* [2019]. For a steady-state case (i.e., the case where there is no time-dependence), the ETRHEQ condition simplifies to

$$\left.\frac{\partial[(r_s(g_s) - r)^2]}{\partial g_s}\right|_{\hat{g}_s} = 0 \tag{S16}$$

Substituting equation S14 into the steady-state ETRHEQ condition (equation S16) and simplifying gives

$$\hat{g}_s = \frac{g_a}{1 + \frac{\lambda \rho g_a q^*(\theta)}{\epsilon(R_n - G)}(1 + \epsilon r)} \frac{r}{1 - r} \tag{S17}$$

Setting the two equations for g_s (equations S11 and S17) equal to one another and solving for H gives

$$H = \frac{c_p q^*(\theta)(R_n - G)}{\Delta\lambda q_a + c_p q^*(\theta)} \tag{S18}$$

Rearranging this gives an expression for the Bowen ratio

$$B \equiv \frac{H}{\lambda E} = \frac{c_p}{r\lambda\Delta} = \frac{R_v c_p T_a^2}{\lambda^2 q_a} \tag{S19}$$

This is identical to the SFE estimate in equation 1 of the main text.

Transient case

In the real-world, there is a strong diurnal cycle, particularly in temperature and available energy, which violates the assumption of steady-state made above. How does this impact the estimate of B? First, note that the ETRHEQ condition (eq. S15) can be rewritten as

$$\frac{1}{T}\int_0^T \frac{\partial}{\partial g_s}\left[(r_s(t, g_s) - r(t))^2\right] dt\Big|_{\hat{g}_s} = 0 \tag{S20}$$

since g_s is treated as constant over the course of one day in ETRHEQ. In general, the time-dependence makes this expression difficult to integrate exactly. Instead, we seek an approximate solution to eq. S20 and show that this solution is very similar to eq. S19 over a wide range of conditions; this implies that eq. S19 should be accurate, even under transient conditions.

The Mean Value Theorem (MVT) for integrals states that, for a function $f(t)$ that is continuous and differentiable over the interval $[a, b]$, there exists some value t_c in the interval $[a, b]$ such that

$$\int_a^b f(t)dt = f(t_c)(b - a) \tag{S21}$$

Applying the MVT to the integral in the ETRHEQ condition (eq. S20) implies that there must exist some time t_c in the interval $[0, T]$ such that

$$\frac{1}{T}\int_0^T \frac{\partial}{\partial g_s}\left[(r_s(t, g_s) - r(t))^2\right] dt = \frac{\partial}{\partial g_s}\left[(r_s(t_c, g_s) - r(t_c))^2\right] \tag{S22}$$

This means that the ETRHEQ condition (eq. S20) can be rewritten as

$$\frac{\partial}{\partial g_s}\left[(r_s(t_c, g_s) - r(t_c))^2\right]\Big|_{\hat{g}_s} = 0 \tag{S23}$$

The advantage of applying the MVT is that we replace an integral which cannot be solved analytically, with an algebraic expression that can be easily manipulated. The price we pay is that the algebraic expression includes the variable t_c which is unknown (although it lies within the interval $[0, T]$).

We now use equation S23 to extend the derivation provided in the previous section to the transient case. Substituting equation S14 into equation S23 and simplifying gives

$$\hat{g}_s = \frac{g_a}{1 + \frac{\lambda\rho g_a q^*(T_M(t_c))}{\epsilon(R_n(t_c) - G(t_c))}(1 + \epsilon(t_c)r(t_c))} \frac{r(t_c)}{1 - r(t_c)} \tag{S24}$$

Recall that, even for the transient case, ETRHEQ continues to treat g_s as constant over the course of one day [*Salvucci and Gentine*, 2013; *Rigden and Salvucci*, 2015]. This implies that the Penman-Monteith solution for g_s applies at all times over the course of the day, including at $t = t_c$. Therefore, setting equation S11 (evaluated at $t = t_c$) equal to equation S24 gives

$$B(t_c) = \frac{R_v c_p T_a^2(t_c)}{\lambda^2 q_a(t_c)} \tag{S25}$$

The key difference between equations S19 and S25 is the latter is evaluated at the unknown time $t = t_c$. The dependence on the unknown t_c is unwanted. To isolate the dependence on t_c, we approximate the Bowen ratio as a constant value during daytime conditions for any given day ($B(t_c) \approx B$), a conventional first-order approximation. The equation is then rewritten as

$$B = \Lambda(t_c) \frac{R_v c_p \overline{T_a}^2}{\lambda^2 \overline{q_a}} \tag{S26}$$

where $\overline{X}$ denotes the daily mean value of X, and

$$\Lambda(t_c) \equiv \frac{\overline{q_a}}{q_a(t_c)} \left(\frac{T_a(t_c)}{\overline{T_a}} \right)^2$$

Since t_c is, by definition, unknown and will vary across sites and individual days, $\Lambda(t_c)$ can be thought of as a random variable. We characterize its distribution across 83 sites at which sufficient observations were available, by estimating it for all possible values of t_c. The estimated mean of Λ is very close to one, both across sites and at each individual site (Fig. S7), with limited variability around this mean value. This confirms that applying equation 1 to transient, real-world cases, in which diurnal variability is significant, is not expected to substantially reduce the accuracy of equation 1. It extends previous work [*McColl et al.*, 2019] on an idealized steady case to the diurnally-varying, transient case.

References

Anthoni, P. M., A. Knohl, C. Rebmann, A. Freibauer, M. Mund, W. Ziegler, O. Kolle, and E.-D. Schulze (2004), Forest and agricultural land-use-dependent CO2 exchange in Thuringia, Germany, *Global Change Biology*, *10*(12), 2005–2019, doi:10.1111/j.1365-2486.2004.00863.x.

Ardo, J., M. Molder, B. A. El-Tahir, and H. A. M. Elkhidir (2008), Seasonal variation of carbon fluxes in a sparse savanna in semi arid Sudan, *Carbon Balance and Management*, *3*(1), 7, doi:10.1186/1750-0680-3-7.

Barr, A., and A. T. Black (2018), Ameriflux ca-sj2 saskatchewan - western boreal, jack pine forest harvested in 2002 from 2003-present, doi:10.17190/AMF/1436321.

Bergeron, O., H. A. Margolis, T. A. Black, C. Coursolle, A. L. Dunn, A. G. Barr, and S. C. Wofsy (2007), Comparison of carbon dioxide fluxes over three boreal black spruce forests in canada, *Global Change Biology*, *13*(1), 89–107, doi:10.1111/J.1365-2486.2006.01281.X.

Beringer, J., L. B. Hutley, J. M. Hacker, B. Neininger, and K. T. P. U (2011), Patterns and processes of carbon, water and energy cycles across northern Australian landscapes: From point to region, *Agricultural and Forest Meteorology*, *151*(11), 1409–1416, doi:10.1016/j.agrformet.2011.05.003.

Bernhofer, C., T. Grunwald, U. Moderow, M. Hehn, U. Eichelmann, and H. Prasse (2016), Fluxnet2015 de-obe oberbarenburg from 2008-2014, doi:10.18140/FLX/1440151.

Bowling, D. R., S. Bethers-Marchetti, C. K. Lunch, E. E. Grote, and J. Belnap (2010), Carbon, water, and energy fluxes in a semiarid cold desert grassland during and following multiyear drought, *Journal of Geophysical Research: Biogeosciences*, *115*(4), doi:10.1029/2010JG001322.

Brunsell, N. (2016a), Ameriflux us-kfs kansas field station from 2007-present, doi:10.17190/AMF/1246132.

Brunsell, N. (2016b), AmeriFlux US-KLS Kansas Land Institute from 2012-, doi:10.17190/AMF/1498745.

Brunsell, N. (2016c), Ameriflux us-kon konza prairie lter (knz) from 2006-present, doi:10.17190/AMF/1246068.

Cernusak, L. A., L. B. Hutley, J. Beringer, J. A. Holtum, and B. L. Turner (2011), Photosynthetic physiology of eucalypts along a sub-continental rainfall gradient in

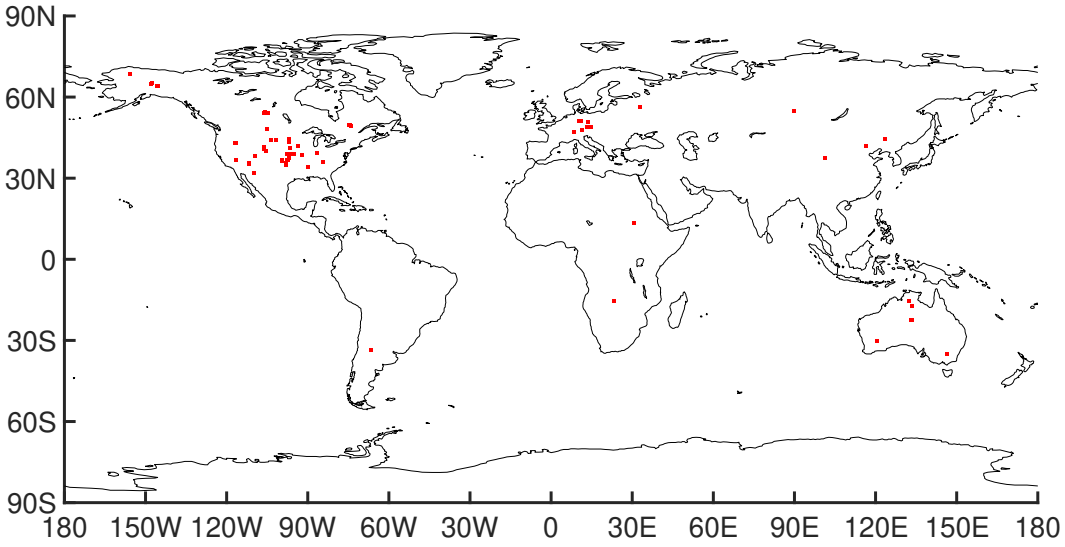

Figure S1. Locations of the 76 Ameriflux and FLUXNET eddy covariance sites used in this study. Further information is provided in Tables S1 and S2.

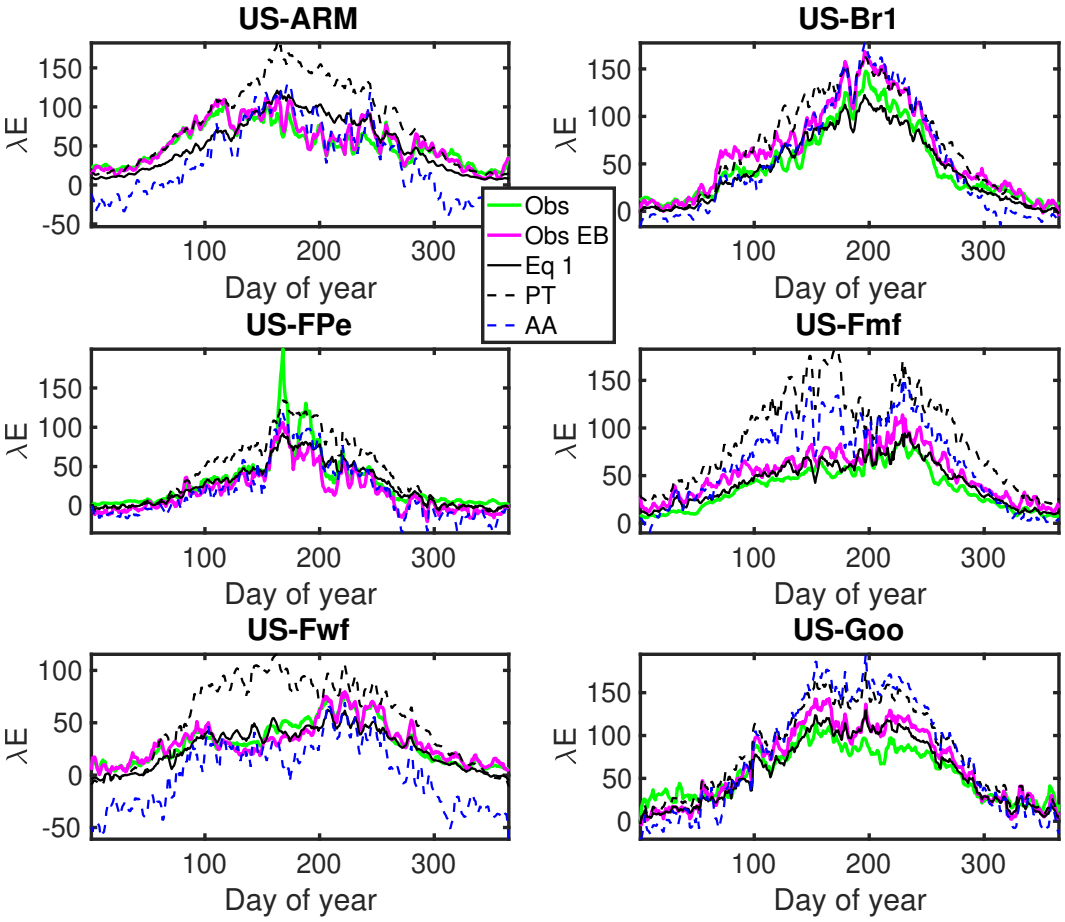

Figure S2. Same as Fig. 3, except for six different sites.

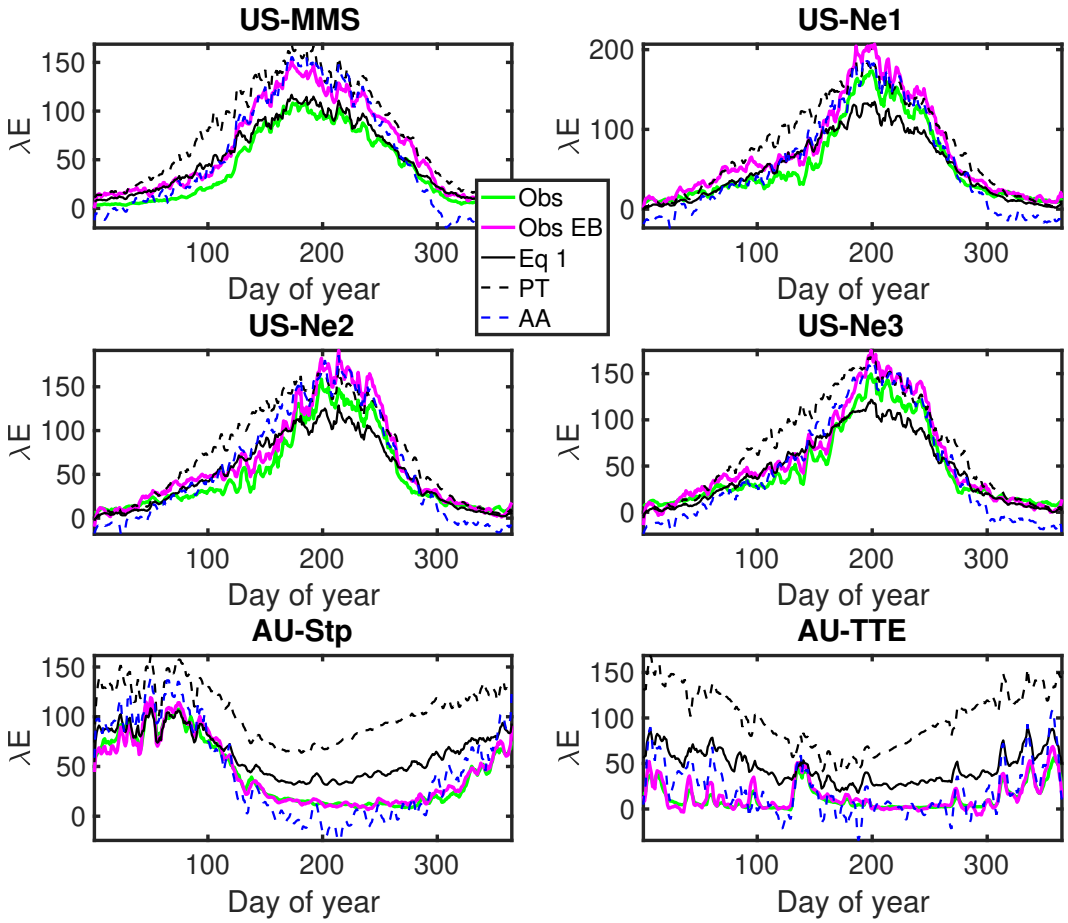

Figure S3. Same as Fig. 3, except for six different sites.

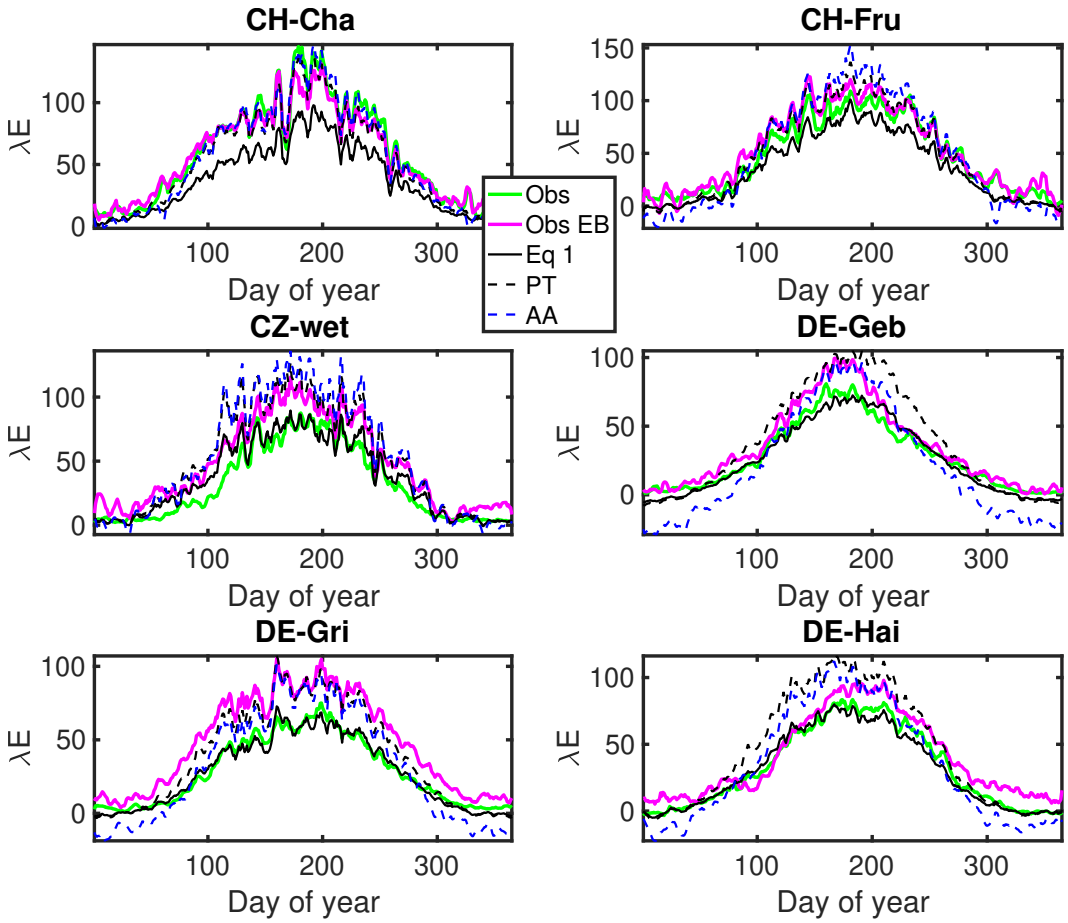

Figure S4. Same as Fig. 3, except for six different sites.

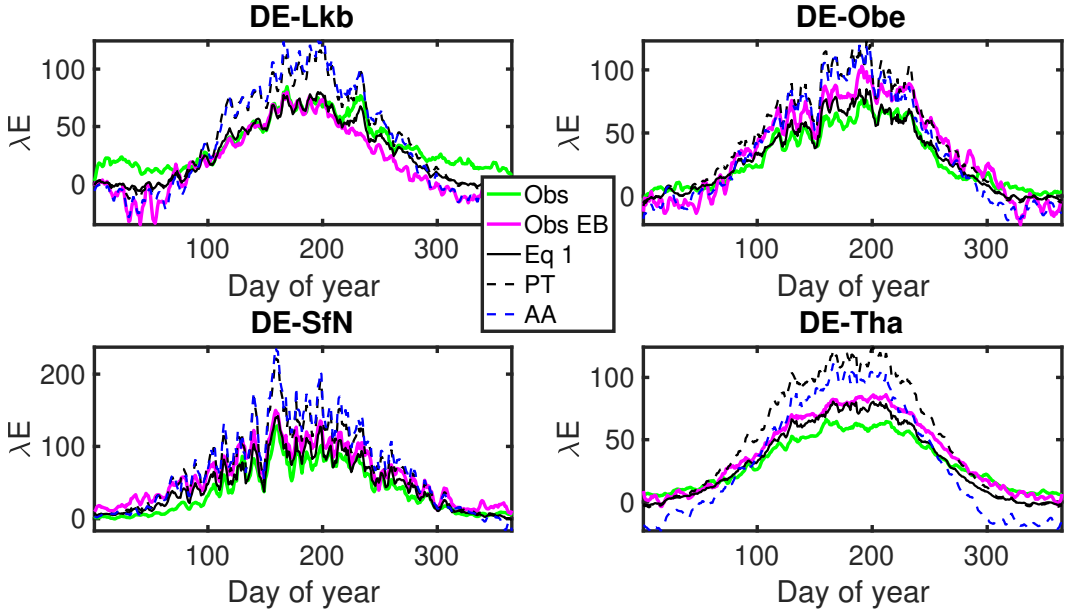

Figure S5. Same as Fig. 3, except for four different sites.

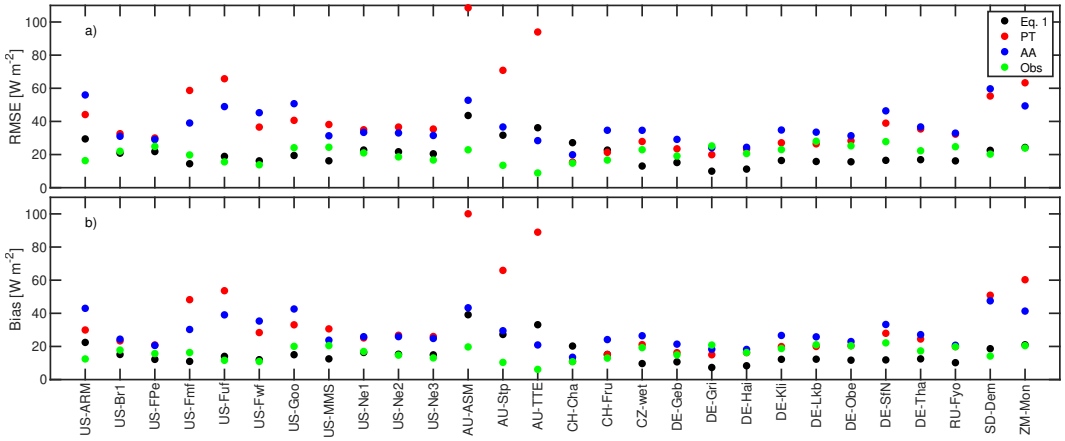

Figure S6. Daily error statistics at the 28 sites plotted in Fig. 3 and Figs. S2-S5: root-mean-squared error (RMSE; a), and mean bias (b). Errors were estimated for equation 1 (black dots), the Priestley-Taylor equation (red dots), and the Advection-Aridity equation (blue dots) by comparing predictions with direct eddy-covariance measurements of λE. For comparison, an estimate of the eddy covariance surface energy budget closure error is provided (green dots), obtained by estimating λE as the residual of the eddy covariance surface energy budget, and then comparing this with direct measurements of λE. Sites are labelled on the horizontal axis. Full details of each site are provided in Tables S1 and S2.

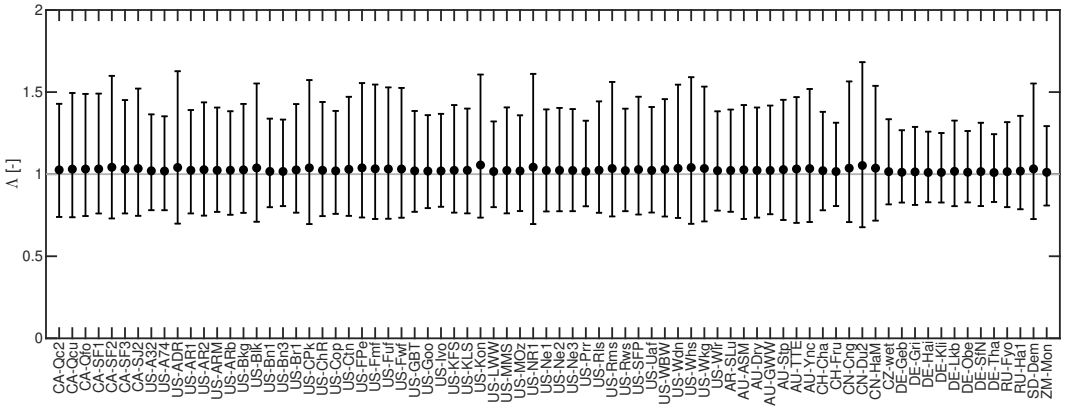

Figure S7. Estimated Λ from observations at the 76 eddy covariance sites used in this study. Specific humidity observations below a noise floor of 5×10^{-4} [kg kg^{-1}] were removed before estimating Λ. Error bars show 95% confidence intervals. The grey horizontal line shows the case where $\Lambda = 1$, the value used in equation 1.

Table S1. Locations and studied periods of Ameriflux eddy covariance sites used in this analysis. All data gathered from www.ameriflux.lbl.gov.

Site name	Latitude	Longitude	Period	Reference
CA-Qc2	49.7598	-74.5711	2007-2010	[*Margolis*, 2018]
CA-Qcu	49.2671	-74.0365	2001-2010	[*Margolis*, 2016]
CA-Qfo	49.6925	-74.3421	2003-2010	[*Bergeron et al.*, 2007]
CA-SF1	54.4850	-105.8176	2003-2006	[*Mkhabela et al.*, 2009]
CA-SF2	54.2539	-105.8775	2001-2006	[*Mkhabela et al.*, 2009]
CA-SF3	54.0916	-106.0053	2001-2006	[*Mkhabela et al.*, 2009]
CA-SJ2	53.9450	-104.6490	2002-2010	[*Barr and Black*, 2018]
US-A32	36.8193	-97.8198	2015-2017	[*Kueppers et al.*, 2018a]
US-A74	36.8085	-97.5489	2015-2017	[*Kueppers et al.*, 2018b]
US-ADR	36.7653	-116.6933	2011-2017	[*Moreo*, 2018]
US-AR1	36.4267	-99.4200	2009-2012	[*Raz-Yaseef et al.*, 2015a]
US-AR2	36.6358	-99.5975	2009-2012	[*Raz-Yaseef et al.*, 2015b]
US-ARb	35.5497	-98.0402	2005-2006	[*Raz-Yaseef et al.*, 2015c]
US-ARM	36.6058	-97.4888	2003-2018	[*Fischer et al.*, 2007]
US-Bkg	44.3453	-96.8362	2004-2010	[*Meyers*, 2016a]
US-Blk	44.1580	-103.6500	2004-2008	[*Meyers*, 2016b]
US-Bn1	63.9198	-145.3782	2002-2004	[*Liu and Randerson*, 2008]
US-Bn3	63.9227	-145.7442	2002-2004	[*Liu and Randerson*, 2008]
US-Br1	41.9749	-93.6906	2005-2011	[*Prueger and Parkin*, 2016]
US-ChR	35.9311	-84.3324	2005-2010	[*Meyers*, 2016c]
US-Cop	38.0900	-109.3900	2001-2007	[*Bowling et al.*, 2010]
US-CPk	41.0680	-106.1187	2009-2013	[*Ewers et al.*, 2016]
US-Ctn	43.9500	-101.8466	2006-2009	[*Meyers*, 2016d]
US-Fmf	35.1426	-111.7273	2005-2010	[*Dore and Kolb*, 2016a]
US-FPe	48.3077	-105.1019	2000-2008	[*Meyers*, 2016e]
US-Fuf	35.0890	-111.7620	2005-2010	[*Dore and Kolb*, 2016b]
US-Fwf	35.4454	-111.7718	2005-2010	[*Dore and Kolb*, 2016c]
US-GBT	41.3658	-106.2397	1999-2006	[*Zeller and Nikolov*, 2000]
US-Goo	34.2547	-89.8735	2002-2006	[*Meyers*, 2018a]
US-Ivo	68.4865	-155.7503	2003-2016	[*Zona and Oechel*, 2018]
US-KFS	39.0561	-95.1907	2007-2012	[*Brunsell*, 2016a]
US-KLS	38.7745	-97.5684	2012-	[*Brunsell*, 2016b]
US-Kon	39.0824	-96.5603	2006-2012	[*Brunsell*, 2016c]
US-LWW	34.9604	-97.9789	1997-1998	[*Meyers*, 2018b]
US-MMS	39.3232	-86.4131	1999-2018	[*Dragoni et al.*, 2011]
US-MOz	38.7441	-92.2000	2004-2015	[*Wood and Gu*, 2016]
US-Ne1	41.1651	-96.4766	2001-2013	[*Verma et al.*, 2005a]
US-Ne2	41.1649	-96.4701	2001-2013	[*Verma et al.*, 2005b]
US-Ne3	41.1797	-96.4397	2001-2013	[*Verma et al.*, 2005c]
US-NR1	40.0329	-105.5464	1998-2014	[*Monson et al.*, 2002]
US-Prr	65.1237	-147.4876	2010-2014	[*Nakai et al.*, 2013]
US-Rls	43.1439	-116.7356	2014-2017	[*Flerchinger et al.*, 2019]
US-Rms	43.0645	-116.7486	2014-2017	[*Flerchinger et al.*, 2019]
US-Rws	43.1675	-116.7132	2014-2017	[*Flerchinger et al.*, 2019]
US-SFP	43.2408	-96.9020	2007-2009	[*Meyers*, 2016f]
US-Uaf	64.8663	-147.8555	2003-2016	[*Iwata et al.*, 2018]
US-WBW	35.9588	-84.2874	1995-2007	[*Meyers*, 2016g]
US-Wdn	40.7838	-106.2618	2006-2008	[*Ewers and Pendall*, 2016]
US-Whs	31.7438	-110.0522	2007-2017	[*Scott et al.*, 2015]
US-Wkg	31.7365	-109.9419	2004-2017	[*Scott et al.*, 2010]
US-Wlr	37.5208	-96.8550	2001-2004	[*Cook and Coulter*, 2016]

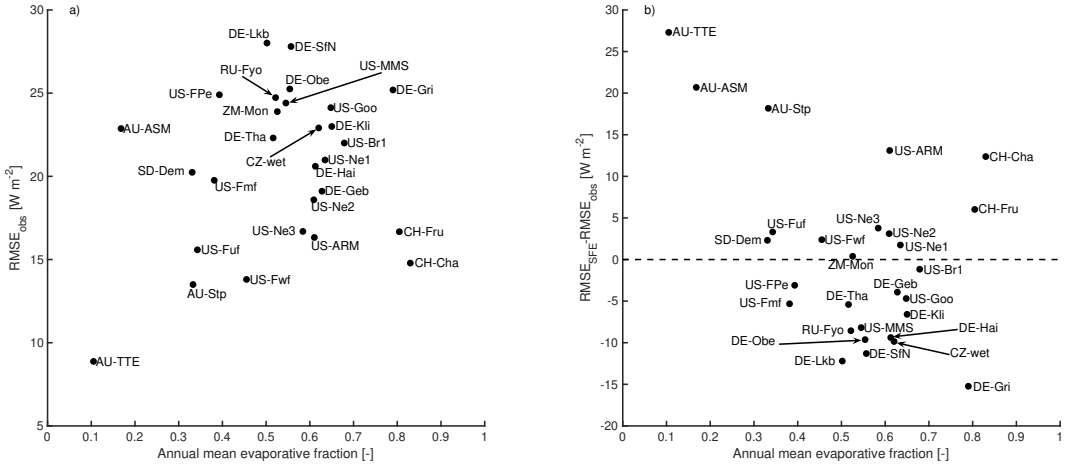

Figure S8. a) Relation between annual mean evaporative fraction and $\mathrm{RMSE_{obs}}$, the root-mean-squared difference between direct eddy covariance measurements of λE, and an alternative estimate obtained by calculating λE as the residual of the eddy covariance surface energy budget. b) Relation between annual mean evaporative fraction and the difference between $\mathrm{RMSE_{obs}}$ and $\mathrm{RMSE_{SFE}}$, the root-mean-squared difference between direct eddy covariance measurements of λE, and the corresponding SFE prediction. Negative values indicate SFE has lower prediction errors than those in the eddy covariance measurements. Full details of each site are provided in Tables S1 and S2.

Table S2. Locations and studied periods of FLUXNET eddy covariance sites used in this analysis. All data gathered from www.fluxdata.org. Duplicates with the Ameriflux database listed in Table 1 are not included here.

Site name	Latitude	Longitude	Period	Reference
AR-SLu	-33.4648	-66.4598	2009-2011	[*Ulke et al.*, 2015]
AU-ASM	-22.2830	133.2490	2010-2013	[*Cleverly et al.*, 2013]
AU-Dry	-15.2588	132.3706	2008-2014	[*Cernusak et al.*, 2011]
AU-GWW	-30.1913	120.6541	2013-2014	[*Prober et al.*, 2012]
AU-Stp	-17.1507	133.3502	2008-2014	[*Beringer et al.*, 2011]
AU-TTE	-22.2870	133.6400	2012-2013	[*Cleverly et al.*, 2016]
AU-Ync	-34.9893	146.2907	2012-2014	[*Yee et al.*, 2015]
CH-Cha	47.2102	8.4104	2005-2014	[*Merbold et al.*, 2014]
CH-Fru	47.1158	8.5378	2005-2014	[*Imer et al.*, 2013]
CN-Cng	44.5934	123.5092	2007-2010	[*Dong*, 2016]
CN-Du2	42.0467	116.2836	2006-2008	[*Chen et al.*, 2009]
CN-HaM	37.3700	101.1800	2002-2004	[*Kato et al.*, 2006]
CZ-wet	49.0247	14.7704	2006-2014	[*Dušek et al.*, 2012]
DE-Geb	51.1001	10.9143	2001-2014	[*Anthoni et al.*, 2004]
DE-Gri	50.9500	13.5126	2004-2014	[*Prescher et al.*, 2010a]
DE-Hai	51.0792	10.4530	2000-2012	[*Knohl et al.*, 2003]
DE-Kli	50.8931	13.5224	2004-2014	[*Prescher et al.*, 2010b]
DE-Lkb	49.0996	13.3047	2009-2013	[*Lindauer et al.*, 2014]
DE-Obe	50.7867	13.7213	2008-2014	[*Bernhofer et al.*, 2016]
DE-SfN	47.8064	11.3275	2012-2014	[*Hommeltenberg et al.*, 2014]
DE-Tha	50.9624	13.5652	1996-2014	[*Grünwald and Bernhofer*, 2007]
RU-Fyo	56.4615	32.9221	1998-2014	[*Kurbatova et al.*, 2008]
RU-Ha1	54.7252	90.0022	2002-2004	[*Marchesini et al.*, 2007]
SD-Dem	13.2829	30.4783	2005-2009	[*Ardo et al.*, 2008]
ZM-Mon	-15.4378	23.2528	2000-2009	[*Merbold et al.*, 2009]

northern Australia, *Agricultural and Forest Meteorology*, *151*(11), 1462–1470, doi: 10.1016/j.agrformet.2011.01.006.

Chen, S., J. Chen, G. Lin, W. Zhang, H. Miao, L. Wei, J. Huang, and X. Han (2009), Energy balance and partition in Inner Mongolia steppe ecosystems with different land use types, *Agricultural and Forest Meteorology*, *149*(11), 1800–1809, doi: 10.1016/j.agrformet.2009.06.009.

Cleverly, J., N. Boulain, R. Villalobos-Vega, N. Grant, R. Faux, C. Wood, P. G. Cook, Q. Yu, A. Leigh, and D. Eamus (2013), Dynamics of component carbon fluxes in a semi-arid Acacia woodland, central Australia, *Journal of Geophysical Research: Biogeosciences*, *118*(3), 1168–1185, doi:10.1002/jgrg.20101.

Cleverly, J., D. Eamus, E. Van Gorsel, C. Chen, R. Rumman, Q. Luo, N. R. Coupe, L. Li, N. Kljun, R. Faux, Q. Yu, and A. Huete (2016), Productivity and evapotranspiration of two contrasting semiarid ecosystems following the 2011 global carbon land sink anomaly, *Agricultural and Forest Meteorology*, *220*, 151–159, doi: 10.1016/j.agrformet.2016.01.086.

Cook, D., and R. L. Coulter (2016), Ameriflux us-wlr walnut river watershed (smileyburg) from 2001-2004, doi:10.17190/AMF/1246115.

Dong, G. (2016), Fluxnet2015 cn-cng changling from 2007-2010, doi: 10.18140/FLX/1440209.

Dore, S., and T. Kolb (2016a), Ameriflux us-fmf flagstaff - managed forest from 2006-2010, doi:10.17190/AMF/1246050.

Dore, S., and T. Kolb (2016b), Ameriflux us-fuf flagstaff - unmanaged forest from 2006-2010, doi:10.17190/AMF/1246051.

Dore, S., and T. Kolb (2016c), Ameriflux us-fwf flagstaff - wildfire from 2006-2010, doi: 10.17190/AMF/1246052.

Dragoni, D., H. P. Schmid, C. A. Wayson, H. Potter, C. S. B. Grimmond, and J. C. Randolph (2011), Evidence of increased net ecosystem productivity associated with a longer vegetated season in a deciduous forest in south-central {I}ndiana, {USA}, *Global Change Biology*, *17*(2), 886–897, doi:10.1111/j.1365-2486.2010.02281.x.

Dušek, J., H. Čížková, S. Stellner, R. Czerný, and J. Květ (2012), Fluctuating water table affects gross ecosystem production and gross radiation use efficiency in a sedge-grass marsh, *Hydrobiologia*, *692*(1), 57–66, doi:10.1007/s10750-012-0998-z.

Ewers, B., and E. Pendall (2016), Ameriflux us-wdn walden from 2006-2008, doi: 10.17190/AMF/1246832.

Ewers, B., E. Pendall, and D. Reed (2016), Ameriflux us-cpk chimney park from 2009-present, doi:10.17190/AMF/1246150.

Fischer, M. L., D. P. Billesbach, J. A. Berry, W. J. Riley, and M. S. Torn (2007), Spatiotemporal variations in growing season exchanges of co2, h2o, and sensible heat in agricultural fields of the southern great plains, *Earth Interactions*, *11*(17), 1–21, doi: 10.1175/EI231.1.

Flerchinger, G. N., A. W. Fellows, M. S. Seyfried, P. E. Clark, and K. A. Lohse (2019), Water and Carbon Fluxes Along an Elevational Gradient in a Sagebrush Ecosystem, *Ecosystems*, doi:10.1007/s10021-019-00400-x.

Grünwald, T., and C. Bernhofer (2007), A decade of carbon, water and energy flux measurements of an old spruce forest at the Anchor Station Tharandt, *Tellus B*, *59*(3), doi: 10.3402/tellusb.v59i3.17000.

Hommeltenberg, J., H. P. Schmid, M. Drösler, and P. Werle (2014), Can a bog drained for forestry be a stronger carbon sink than a natural bog forest?, *Biogeosciences*, *11*(13), 3477–3493, doi:10.5194/bg-11-3477-2014.

Imer, D., L. Merbold, W. Eugster, and N. Buchmann (2013), Temporal and spatial variations of soil CO_2, CH_4 and N_2O fluxes at three differently managed grasslands, *Biogeosciences*, *10*(9), 5931–5945, doi:10.5194/bg-10-5931-2013.

Iwata, H., M. Ueyama, and Y. Harazono (2018), Ameriflux us-uaf university of alaska, fairbanks from 2002-present, doi:10.17190/AMF/1480322.

Kato, T., Y. Tang, S. Gu, M. Hirota, M. Du, Y. Li, and X. Zhao (2006), Temperature and biomass influences on interannual changes in CO2 exchange in an alpine meadow on the Qinghai-Tibetan Plateau, *Global Change Biology*, *12*(7), 1285–1298, doi:10.1111/j.1365-2486.2006.01153.x.

Knohl, A., E.-D. Schulze, O. Kolle, and N. Buchmann (2003), Large carbon uptake by an unmanaged 250-year-old deciduous forest in central Germany, *Agricultural and Forest Meteorology*, *118*(3-4), 151–167, doi:10.1016/s0168-1923(03)00115-1.

Kueppers, L., M. Torn, and S. Biraud (2018a), Ameriflux us-a32 arm-sgp medford hay pasture from 2015-present, doi:10.17190/AMF/1436327.

Kueppers, L., M. Torn, and S. Biraud (2018b), Ameriflux us-a74 arm sgp milo field from 2016-present, doi:10.17190/AMF/1436328.

Kurbatova, J., C. Li, A. Varlagin, X. Xiao, and N. Vygodskaya (2008), Modeling carbon dynamics in two adjacent spruce forests with different soil conditions in Russia, *Biogeosciences*, *5*(4), 969–980, doi:10.5194/bg-5-969-2008.

Lindauer, M., H. Schmid, R. Grote, M. Mauder, R. Steinbrecher, and B. Wolpert (2014), Net ecosystem exchange over a non-cleared wind-throw-disturbed upland spruce forest—measurements and simulations, *Agricultural and Forest Meteorology*, *197*, 219–234, doi:10.1016/j.agrformet.2014.07.005.

Liu, H., and J. T. Randerson (2008), Interannual variability of surface energy exchange depends on stand age in a boreal forest fire chronosequence, *Journal of Geophysical Research: Biogeosciences*, *113*(G1), doi:10.1029/2007JG000483.

Marchesini, L. B., D. Papale, M. Reichstein, N. Vuichard, N. Tchebakova, and R. Valentini (2007), Carbon balance assessment of a natural steppe of southern Siberia by multiple constraint approach, *Biogeosciences Discussions*, *4*(1), 165–208, doi:10.5194/bgd-4-165-2007.

Margolis, H. (2018), Ameriflux ca-qc2 quebec - 1975 harvested black spruce (hbs75) from 2007-present, doi:10.17190/AMF/1419514.

Margolis, H. A. (2016), Ameriflux ca-qcu quebec - eastern boreal, black spruce/jack pine cutover from 2001-present, doi:10.17190/AMF/1246828.

McColl, K. A., G. D. Salvucci, and P. Gentine (2019), Surface flux equilibrium theory explains an empirical estimate of water-limited daily evapotranspiration, *Journal of Advances in Modeling Earth Systems*, *11*(7), 2036–2049.

Merbold, L., J. Ardö, A. Arneth, R. J. Scholes, Y. Nouvellon, A. de Grandcourt, S. Archibald, J. M. Bonnefond, N. Boulain, N. Brueggemann, C. Bruemmer, B. Cappelaere, E. Ceschia, H. A. M. El-Khidir, B. A. El-Tahir, U. Falk, J. Lloyd, L. Kergoat, V. L. Dantec, E. Mougin, M. Muchinda, M. M. Mukelabai, D. Ramier, O. Roupsard, F. Timouk, E. M. Veenendaal, and W. L. Kutsch (2009), Precipitation as driver of carbon fluxes in 11 African ecosystems, *Biogeosciences*, *6*(6), 1027–1041, doi:10.5194/bg-6-1027-2009.

Merbold, L., W. Eugster, J. Stieger, M. Zahniser, D. Nelson, and N. Buchmann (2014), Greenhouse gas budget (CO2, CH4and N2O) of intensively managed grassland following restoration, *Global Change Biology*, *20*(6), 1913–1928, doi:10.1111/gcb.12518.

Meyers, T. (2016a), Ameriflux us-bkg brookings from 2004-present, doi:10.17190/AMF/1246040.

Meyers, T. (2016b), Ameriflux us-blk black hills from 2003-2008, doi:10.17190/AMF/1246031.

Meyers, T. (2016c), Ameriflux us-chr chestnut ridge from 2005-present, doi:10.17190/AMF/1246044.

Meyers, T. (2016d), Ameriflux us-ctn cottonwood from 2007-2009, doi:10.17190/AMF/1246117.

Meyers, T. (2016e), Ameriflux us-fpe fort peck from 2000-present, doi:10.17190/AMF/1246053.

Meyers, T. (2016f), Ameriflux us-sfp sioux falls portable from 2007-present, doi:10.17190/AMF/1246126.

Meyers, T. (2016g), Ameriflux us-wbw walker branch watershed from 1995-1999, doi: 10.17190/AMF/1246109.

Meyers, T. (2018a), Ameriflux us-goo goodwin creek from 2002-2006, doi: 10.17190/AMF/1246058.

Meyers, T. (2018b), Ameriflux us-lww little washita watershed from 1997-1998, doi: 10.17190/AMF/1246073.

Mkhabela, M., B. Amiro, A. Barr, T. Black, I. Hawthorne, J. Kidston, J. McCaughey, A. Orchansky, Z. Nesic, A. Sass, A. Shashkov, and T. Zha (2009), Comparison of carbon dynamics and water use efficiency following fire and harvesting in canadian boreal forests, *Agricultural and Forest Meteorology*, *149*(5), 783–794, doi: 10.1016/J.AGRFORMET.2008.10.025.

Monson, R. K., A. A. Turnipseed, J. P. Sparks, P. C. Harley, L. E. Scott-Denton, K. Sparks, and T. E. Huxman (2002), Carbon sequestration in a high-elevation, subalpine forest, *Global Change Biology*, *8*(5), 459–478, doi:10.1046/J.1365-2486.2002.00480.X.

Moreo, M. (2018), Ameriflux us-adr amargosa desert research site (adrs) from 2011-present, doi:10.17190/AMF/1418680.

Nakai, T., Y. Kim, R. C. Busey, R. Suzuki, S. Nagai, H. Kobayashi, H. Park, K. Sugiura, and A. Ito (2013), Characteristics of evapotranspiration from a permafrost black spruce forest in interior alaska, *Polar Science*, *7*(2), 136–148, doi: 10.1016/J.POLAR.2013.03.003.

Prescher, A.-K., T. Grünwald, and C. Bernhofer (2010a), Land use regulates carbon budgets in eastern Germany: From NEE to NBP, *Agricultural and Forest Meteorology*, *150*(7-8), 1016–1025, doi:10.1016/j.agrformet.2010.03.008.

Prescher, A.-K., T. Grünwald, and C. Bernhofer (2010b), Land use regulates carbon budgets in eastern germany: From NEE to NBP, *Agricultural and Forest Meteorology*, *150*(7-8), 1016–1025, doi:10.1016/j.agrformet.2010.03.008.

Prober, S. M., K. R. Thiele, P. W. Rundel, C. J. Yates, S. L. Berry, M. Byrne, L. Christidis, C. R. Gosper, P. F. Grierson, K. Lemson, T. Lyons, C. Macfarlane, M. H. O'Connor, J. K. Scott, R. J. Standish, W. D. Stock, E. J. van Etten, G. W. Wardell-Johnson, and A. Watson (2012), Facilitating adaptation of biodiversity to climate change: A conceptual framework applied to the world's largest Mediterranean-climate woodland, *Climatic Change*, *110*(1-2), 227–248, doi:10.1007/s10584-011-0092-y.

Prueger, J., and T. Parkin (2016), Ameriflux us-br1 brooks field site 10- ames from 2001-present, doi:10.17190/AMF/1246038.

Raz-Yaseef, N., D. P. Billesbach, M. L. Fischer, S. C. Biraud, S. A. Gunter, J. A. Bradford, and M. S. Torn (2015a), Vulnerability of crops and native grasses to summer drying in the {U.S.} Southern {G}reat {P}lains, *Agriculture, Ecosystems & Environment*, *213*, 209–218, doi:10.1016/j.agee.2015.07.021.

Raz-Yaseef, N., D. P. Billesbach, M. L. Fischer, S. C. Biraud, S. A. Gunter, J. A. Bradford, and M. S. Torn (2015b), Vulnerability of crops and native grasses to summer drying in the {U.S.} Southern {G}reat {P}lains, *Agriculture, Ecosystems & Environment*, *213*, 209–218, doi:10.1016/j.agee.2015.07.021.

Raz-Yaseef, N., D. P. Billesbach, M. L. Fischer, S. C. Biraud, S. A. Gunter, J. A. Bradford, and M. S. Torn (2015c), Vulnerability of crops and native grasses to summer drying in the {U.S. S}outhern {G}reat {P}lains, *Agriculture, Ecosystems & Environment*, *213*, 209–218, doi:10.1016/j.agee.2015.07.021.

Rigden, A. J., and G. D. Salvucci (2015), Evapotranspiration based on equilibrated relative humidity (ETRHEQ): Evaluation over the continental U.S., *Water Resources Research*, *51*(4), 2951–2973, doi:10.1002/2014WR016072.

Salvucci, G. D., and P. Gentine (2013), Emergent relation between surface vapor conductance and relative humidity profiles yields evaporation rates from weather data, *Proceedings of the National Academy of Sciences*, *110*(16), 6287–6291, doi: 10.1073/pnas.1215844110.

Scott, R. L., E. P. Hamerlynck, G. D. Jenerette, M. S. Moran, and G. A. Barron-Gafford (2010), Carbon dioxide exchange in a semidesert grassland through drought-induced vegetation change, *Journal of Geophysical Research*, *115*(G3), n/a–n/a, doi: 10.1029/2010JG001348.

Scott, R. L., J. A. Biederman, E. P. Hamerlynck, and G. A. Barron-Gafford (2015), The carbon balance pivot point of southwestern u.s. semiarid ecosystems: Insights from the 21st century drought, *Journal of Geophysical Research: Biogeosciences*, *120*(12), 2612–2624, doi:10.1002/2015JG003181.

Ulke, A. G., N. N. Gattinoni, and G. Posse (2015), Analysis and modelling of turbulent fluxes in two different ecosystems in Argentina, *International Journal of Environment and Pollution*, *58*(1/2), 52, doi:10.1504/ijep.2015.076583.

Verma, S. B., A. Dobermann, K. G. Cassman, D. T. Walters, J. M. Knops, T. J. Arkebauer, A. E. Suyker, G. G. Burba, B. Amos, H. Yang, D. Ginting, K. G. Hubbard, A. A. Gitelson, and E. A. Walter-Shea (2005a), Annual carbon dioxide exchange in irrigated and rainfed maize-based agroecosystems, *Agricultural and Forest Meteorology*, *131*(1-2), 77–96, doi:10.1016/j.agrformet.2005.05.003.

Verma, S. B., A. Dobermann, K. G. Cassman, D. T. Walters, J. M. Knops, T. J. Arkebauer, A. E. Suyker, G. G. Burba, B. Amos, H. Yang, D. Ginting, K. G. Hubbard, A. A. Gitelson, and E. A. Walter-Shea (2005b), Annual carbon dioxide exchange in irrigated and rainfed maize-based agroecosystems, *Agricultural and Forest Meteorology*, *131*(1-2), 77–96, doi:10.1016/j.agrformet.2005.05.003.

Verma, S. B., A. Dobermann, K. G. Cassman, D. T. Walters, J. M. Knops, T. J. Arkebauer, A. E. Suyker, G. G. Burba, B. Amos, H. Yang, D. Ginting, K. G. Hubbard, A. A. Gitelson, and E. A. Walter-Shea (2005c), Annual carbon dioxide exchange in irrigated and rainfed maize-based agroecosystems, *Agricultural and Forest Meteorology*, *131*(1-2), 77–96, doi:10.1016/j.agrformet.2005.05.003.

Wood, J., and L. Gu (2016), Ameriflux us-moz missouri ozark site from 2004-present, doi:10.17190/AMF/1246081.

Yee, M. S., V. R. Pauwels, E. Daly, J. Beringer, C. Rüdiger, M. F. McCabe, and J. P. Walker (2015), A comparison of optical and microwave scintillometers with eddy covariance derived surface heat fluxes, *Agricultural and Forest Meteorology*, *213*, 226–239, doi:10.1016/j.agrformet.2015.07.004.

Zeller, K. F., and N. T. Nikolov (2000), Quantifying simultaneous fluxes of ozone, carbon dioxide and water vapor above a subalpine forest ecosystem, *Environmental Pollution*, *107*(1), 1–20, doi:10.1016/S0269-7491(99)00156-6.

Zona, D., and W. Oechel (2018), Ameriflux us-ivo ivotuk from 2003-present, doi: 10.17190/AMF/1246067.